



**Faculty of Electrical Engineering**  
**Department of Control Engineering**

**Bachelor's thesis**

**Locomotion Control  
of Hexapod Walking Robot  
with Four Degrees of Freedom per Leg**

**Martin Zoula**

**May 2019**  
**Supervisor:** Doc. Ing. Jan Faigl, Ph.D.  
**Supervisor specialist:** Ing. Petr Čížek

## I. Personal and study details

Student's name: **Zoula Martin**

Personal ID number: **466113**

Faculty / Institute: **Faculty of Electrical Engineering**

Department / Institute: **Department of Control Engineering**

Study program: **Cybernetics and Robotics**

## II. Bachelor's thesis details

Bachelor's thesis title in English:

**Locomotion Control of Hexapod Walking Robot with Four Degrees of Freedom per Leg**

Bachelor's thesis title in Czech:

**Řízení pohybu šestinohého kráčejícího robotu se čtyřmi řiditelnými stupni volnosti na nohu**

Guidelines:

1. Familiarize yourself with the hexapod walking robot platform of the Computational Robotics Laboratory and its locomotion control [1].
2. Familiarize yourself with multi-legged walking platforms with multiple degrees of freedom per leg, e.g., [2-4].
3. Enhance the hexapod robot walking and manipulation capabilities by adding an actuator into the legs kinematic chain to obtain four degrees of freedom per leg in yaw-roll-pitch-pitch configuration.
4. Deploy the foot-contact detection algorithm and the locomotion gait [1] on the robot.
5. Experimentally verify the enhanced walking capabilities of the developed platform in slope walking [2].

Bibliography / sources:

- [1] J. Mrva, J. Faigl, Tactile sensing with servo drives feedback only for blind hexapod walking robot, *Robot Motion and Control (RoMoCo)*, 2015, pp. 240-245.  
[2] M. Bjelonic, N. Kottege, T. Homberger, P.V. Koerich Borges, P. Beckerle, M. Chli: Weaver: Hexapod robot for autonomous navigation on unstructured terrain. *Journal of Field Robotics* 35(7): 1063-1079, 2018.  
[3] A. Roennau, G. Heppner, M. Nowicki, R. Dillmann: LAURON V: A versatile six-legged walking robot with advanced maneuverability, *IEEE/ASME International Conference on Advanced Intelligent Mechatronics*, 2014, pp. 82-87.  
[4] G. Bledt, M. J. Powell, B. Katz, J. Di Carlo, P. M. Wensing, K. Sangbae: MIT Cheetah 3: Design and Control of a Robust, Dynamic Quadruped Robot, *IEEE/RSJ International Conference on Robots and Systems (IROS)*, 2018, pp. 2245-2252.  
[5] M. W. Spong, S. Hutchinson, M. Vidyasagar: Robot modeling and control. Wiley New York, 2006, John Wiley & Sons, Inc.

Name and workplace of bachelor's thesis supervisor:

**doc. Ing. Jan Faigl, Ph.D., Artificial Intelligence Center, FEE**

Name and workplace of second bachelor's thesis supervisor or consultant:

**Ing. Petr Čížek, Artificial Intelligence Center, FEE**

Date of bachelor's thesis assignment: **24.01.2019** Deadline for bachelor thesis submission: **24.05.2019**

Assignment valid until: **20.09.2020**

---

doc. Ing. Jan Faigl, Ph.D.  
Supervisor's signature

prof. Ing. Michael Šebek, DrSc.  
Head of department's signature

prof. Ing. Pavel Ripka, CSc.  
Dean's signature

### III. Assignment receipt

The student acknowledges that the bachelor's thesis is an individual work. The student must produce his thesis without the assistance of others, with the exception of provided consultations. Within the bachelor's thesis, the author must state the names of consultants and include a list of references.

Date of assignment receipt

Student's signature

## **Declaration**

I declare that the presented work was developed independently and that I have listed all sources of the information used within it in accordance with the methodical instructions for observing the ethical principles in the preparation of university theses.

Prague, May 24, 2019

.....  
Martin Zoula

## Acknowledgement

I would like to thank both my supervisors Petr Čížek and Jan Faigl for assigning me this particular thesis and providing me with regular meaningful consultations despite their tight schedule. During work on this thesis, I was given insight into many problems associated with vast area of mobile robotics which I very value.

I would like to thank my high school teachers who taught me more than is probably expected nowadays. Only with time one recognises importance of deeds past; my secondary school influenced me deeply, not only with knowledge gained, but also with people I got to know.

A konečně bych velmi rád poděkoval své milé rodině, mamince, tatínkovi, bráškovi, babičkám a dědečkům za to nekonečné vše, co pro mne kdy udělali.

## Abstrakt

V této práci představujeme nového šestinohého robota jménem HAntR, kterého jsme vytvořili dle potřeb Laboratoře výpočetní robotiky Centra umělé inteligence fakulty Elektrotechnické Českého vysokého učení technického v Praze. Jeho hlavním účelem jest vylepšit schopnosti pohybu v těžkém terénu původního robota přidáním čtvrtého stupně volnosti každé noze. Na základě nově navržené nohy jsme také přepracovali celé tělo robota tak, aby splnilo i další požadavky, jako například menší rozměry, či možnost osazení alespoň šesti Lithium-Iontovými monočlánky. V práci pečlivě popisujeme motivace a úvahy, které nás k výslednému návrhu vedly. Uvádíme řešení přímé i inverzní kinematické úlohy řešené pomocí podmínky na ideální orientaci konce nohy a uvažující i důležité kinematické singularity. Navržený robot byl vyzkoušen v několika experimentech, při kterých byl použit námi navržený řídicí systém napsaný v jazyce C++. Ukázalo se, že HAntR vydrží díky zvýšené energetické hustotě a lepšímu rozkladu sil v končetinách autonomně fungovat přes hodinu. Robot je také schopen jít rychlostí až  $0.42 \text{ m s}^{-1}$ , což předčí mnohé srovnatelné roboty. Při experimentu, kdy robot stál na nakloněné rovině, bylo prokázáno zlepšení oproti předchozímu robotu. A také jsme dle pokynů této práce potvrdili, že i HAntR je schopen adaptivní chůze spoléhající pouze na poziciální zpětnou vazbu.

**Klíčová slova:** Robotika, Vícenoží kráčející roboti, Hexapod, Kinematika, Mechanický návrh, Adaptivní chůze

## Abstract

In this thesis a novel six-legged robot called HAntR is presented. The robot was developed according to needs of the Robotics Laboratory, at the Artificial Intelligent Center, Faculty of Electrical Engineering, Czech Technical University in Prague. Its main purpose is enhancing rough-terrain movement capabilities by upgrading a former design by adding fourth degree of freedom to each leg. We also revised robot torso to fit new leg design and incorporate other requirements such as smaller dimensions with space for at least six Lithium-Ion cells. We thoroughly describe motivations and considerations that led us to the presented particular solution. Further, the solutions of forward and inverse kinematic tasks with partial orientation constraint and important singularities avoidance are presented. The proposed design has been evaluated in several experimental deployments, which utilised developed software controller written in C++. Endurance tests showed, that HAntR is able to remotely operate for over an hour thanks to increased energy density. Maximal speed test resulted to  $0.42 \text{ m s}^{-1}$  during tripod gait, which outpaces most of the comparable robotic platforms. Experiment where HAntR stood on platform with varying inclination showed qualitative improvement against former robot. Finally, in accord with the thesis assignment, we proved that HAntR is able to perform walking with adaptive gait using positional feedback only.

**Keywords:** Robotics, Multi-legged walking robots, Hexapod, Kinematics, Mechanical design, Adaptive gait

# Contents

<b>1</b>	<b>Introduction</b>	<b>1</b>
1.1	Existing Research on Hexapod Robots . . . . .	3
<b>2</b>	<b>List of Design Specifications</b>	<b>5</b>
<b>3</b>	<b>Proposed Design</b>	<b>8</b>
3.1	Mechanical Design . . . . .	8
3.1.1	Leg . . . . .	10
3.1.2	Torso . . . . .	15
3.1.3	CAD Software and Manufacturing Technology . . . . .	16
3.2	Kinematics and Control . . . . .	18
3.2.1	Direct Kinematic Task . . . . .	20
3.2.2	Inverse Kinematic Task . . . . .	22
3.2.3	Implementation . . . . .	25
<b>4</b>	<b>Verification</b>	<b>26</b>
4.1	Resulting Design . . . . .	26
4.1.1	Verification of Kinematics . . . . .	29
4.2	Foot Strike Detection Using Positional Feedback Only . . . . .	30
4.2.1	Error Threshold Estimation . . . . .	31
4.2.2	Deployment in Locomotion Gait . . . . .	31
4.3	Obtained Properties . . . . .	33
4.3.1	Endurance and Temperature Test . . . . .	33
4.3.2	Maximum Speed Test . . . . .	35
4.3.3	Variable-Steep Slope Adaption Test . . . . .	35
<b>5</b>	<b>Conclusion</b>	<b>39</b>
5.1	Future Work . . . . .	40
	<b>References</b>	<b>42</b>
<b>A</b>	<b>Mechanical Design Blueprints</b>	<b>46</b>
<b>B</b>	<b>Contents of Attached CD</b>	<b>53</b>

## List of Figures

1	Photography of HAntR and PhantomX AX Mark II hexapod robots.	2
2	Renderings of the created CAD models.	8
3	Orthogonal overview drawing of individual mechanical parts.	10
4	Dynamixel AX-12A servomotor.	12
5	Considered existing leg designs.	13
6	Leg-body interface.	15
8	Visualisation of a multi-legged robot mathematical model.	19
9	Computing Femur and Tibia joint coordinates as circle intersection problem.	24
10	Photography of deployed HAntR.	27
11	Possible compact folding of legs.	28
12	IKT-proving experiment.	28
13	Visualisation of HAntR leg operating space.	29
14	Photography of fixed-threshold derivation setup.	30
15	Positional error during single leg footstrike.	32
16	Graph of HAntR torso height during adaptive and non-adaptive walk.	34
17	Photography of HAntR performing treading in place.	34
18	Temperature evolution in individual joints during endurance experiment.	35
19	Image from a camera used for Apriltag localisation.	36
20	Comparison of positional errors during slope balancing.	37
21	Photography of slope balancing experiment.	37

## List of Tables

1	Comparison of selected hexapod robots.	4
2	List of proposed parts.	9
3	Denavit-Hartenberg parameters table.	21
4	Fixed joint coordinates safety limits.	25
5	Building cost of HAntR.	27
6	Derived regulating error thresholds for adaptive gait.	31
7	Seamless tripod gait diagram.	33
8	Results of slope balancing experiment.	36

## List of Abbreviations

ABS	Acrylonitrile Butadiene Styrene	FTP	Femur-Tibia Plane
AHRS	Attitude-Heading Reference System	IKT	Inverse Kinematic Task
CAD	Computer-Aided Design	Li-Ion	Lithium-Ion
ComRob	Computational Robotics Laboratory	Li-Poly	Lithium-Polymer
D-H	Denavit-Hartenberg	P-regulator	Proportional regulator
DKT	Direct Kinematic Task	PLA	Polylactic Acid
DoF	Degree of Freedom	STL	Stereolithography,
			Standard Triangle Language
		w.r.t.	With Respect To

# Chapter 1

## Introduction

With a recent progress of Mankind, a need for *robots* has arised. The term was coined in 1920 by Czech playwright and writer Karel Čapek [1] and originally meant an organic humanoid capable of performing general tasks. Currently, we understand by this term machines controlled by electronic devices, which are built for specific purposes only<sup>1</sup>. Although we know about several universal anthropomorphic robots in popular culture, such as Marvin, Dorfl or Cryten<sup>2</sup>, these robots still remain only in our dreams nowadays. In recent decades, the pool of available robotic platforms has thrived along fast expanding capabilities of electronics.

We can classify robots into two categories: Stationary robots and mobile robots [2]. Stationary robots benefit from rigid connection with their environment, whifch simplifies their kinematic tasks and positioning and makes them more common and widespread. They are used, e.g., in the industry for automation of production processes, where the environment and its character is well-defined beforehand and controlled during operations. On the other hand, mobile robots must deal with the environment changing during runtime, either by their movement or by the environment changing in its own right, making the robot more prone to mechanical failures. The threats can be attenuated by optimised mechanical construction, e.g., as in the case of Curiosity rover [3] or passive walkers [4]. Thus, we can distinguish between several types of robots, e.g., ground, aerial or naval.

This thesis deals with a topic of six-legged walking robots, called in shorthand *hexapods*<sup>3</sup>. It is proven compromise between static stability and mobility because six legs represents the smallest number of legs, which offers *two-stride statically stable gait* [5]. Robots with less legs can also offer static gait, but need to perform more strides per gait cycle to walk so. More legs can increase redundancy [6] or robustness [7] at the cost of increased cost, maintanance, and control complexity. On the other hand, a robot with less legs like biped or quadruped can benefit, e.g., from walking with straightened legs. Such walk is more difficult for control, but offers better energy budget due to the robot weight being supported by passive reactive force rather than by active servomotor effort [4]. Walking with three or more supporting legs cannot be passive; this can even result to standing robot still demanding c.a. the same ammount of power, as if it was walking [8].

Supposed application of hexapod robots could be in multi-robot exploration task where currently minimalist solutions [9] or wheeled robots [10] thrives, in harsh environments where specifically designed solutions [11] are being deployed or quadruped solutions like [12, 13] exists, or as security and maintenance drones deployed in factories or even at oil rigs [14].

Hexapod consists of main body or *torso* and six legs based in various points and orientations on the body. Legs are kinematic structures, possibly designed as open chains with several degrees of freedom (DoF) [2, 15] and articulated by rotating joints. Parallel or mixed kinematic structures are

<sup>1</sup> Nowadays robots are incapable of rational contemplation or General Intelligence. Therefore they cannot obey or defy the Three Laws of Robotics defined by Isaac Asimov or any extension by Ljuben Dilov, Nikola Kesarovski or Roger MacBride Allen from their will and no blame for harm can be directly imposed to them. Instead they still need to be carefully explicitly programmed to comply with these rules or rather with legislation of given country. The question of responsibility related to robotics is nowadays big concern and is being discussed worldwide.

<sup>2</sup> Paranoid android with “head size of a planet” from *The Hitchhiker’s Guide to the Galaxy* by Douglas Adams; golem, a clay-man ruled by a chem containing words of commands, who became self-aware in *Discworld* novel *Feet of Clay* by Terry Pratchett; self-reliant toilet cleaning android from *Red Dwarf* sitcom series, respectively.

<sup>3</sup> There also exist a category of a robotic manipulator utilising six linear actuators, which allow for positioning in all six DoF. In this thesis, by term “hexapod” we will always mean the walking one.

## 1. Introduction

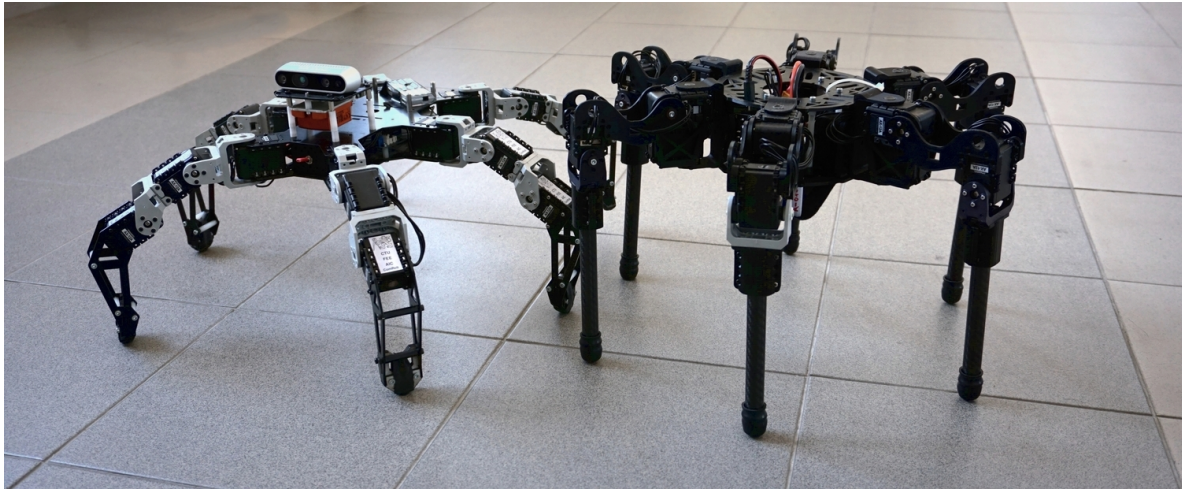


Figure 1: Photography of HAntR and PhantomX AX Mark II hexapod robots.

also possible, but we focused the former mentioned because well-developed theory of Affine spaces and Homogeneous transformations can be utilised. We call the individual joints and respective links according to biological nomenclature of insect leg as Coxa, Trochanter, Femur, Tibia and Tarsus [16–18].

Computational Robotics Laboratory (ComRob)<sup>4</sup> currently uses two types of robots to verify its research in real-world deployments. A fixed-wing aerial drone and multiple PhantomX AX Mark II [19] (further referenced also as PhantomX) hexapods from Trossen Robotics company depicted in Figure 1. The goal of this thesis is to develop a new experimental hexapod robot platform called “HAntR” (standing for Hexapod Ant Robot). The robot has been designed to offer substantial improvements in motion capabilities, reliability, and robustness in comparison to the PhantomX robot, and to allow for autonomous operations including exploration of uncharted areas in data-collection missions in the extraterrestrial, wilderness, or subterranean environments. The main feature of the resulting design was adding a fourth DoF per leg, resulting in an overhaul of the entire former leg design, and finally, improving locomotion capability; the herein proposed design retained only Dynamixel AX-12A servomotors used as joint actuators. Consequently, we had to redesign whole torso and adjust the kinematic model together with the implementation of the adaptive locomotion control.

We write about existing hexapod robots that served as an inspiration for our design in the following Section; several relevant hexapods are described more closely, whereas Table 1 provides a comparison with other hexapods. The design was also motivated by ComRob members five years of experience with the PhantomX robot. Combined with our own ideas, a reader may find resulting list of Specifications in Section 2. In Section 3, the proposed design with material and manufacturing considerations is explained, particularly Section 3.1.1 reports on the design of novel leg, Section 3.1.2 then recounts the design of torso. Afterwards in Section 3.2, when a mechanical design is established, we describe a kinematic model derived from mechanical properties. The robot was finally evaluated in indoor deployment; Section 4 holds information about tests, that verified supposed properties. It was shown, that the robot is indeed better than PhantomX, e.g. in endurance or slope-balancing. We conclude the thesis in Section 5, which also names some of the future possibilities of the robot.

---

<sup>4</sup> Artificial Intelligent Center at the Faculty of Electrical Engineering, Czech Technical University in Prague, member of the Center for Robotics and Autonomous Systems.

## 1.1 Existing Research on Hexapod Robots

The developed robot takes its place among other hexapods [20], which differ by their terrain traversability capabilities, onboard electronic equipment, battery capacity, and corresponding endurance. In this Section, we provide an overview of existing hexapods with properties comparable to HAntR robot.

RHex [21] and derived robots utilise single servomotor per leg, which makes them robust and yet allows them to perform several types of gaits, such as pronking, rearing or trotting. Their joints operate in near-passive pose similarly to wheeled vehicles, which increases their payload weight and endurance. On the other hand, they cannot tackle as rough terrain as other hexapods because of absence of lateral foottip positioning or force control.

Adding one DoF results in robots like Vorpal [31], which has legs in yaw-pitch configuration enabling foottip positioning along a sphere surface. Mentioned robot in particular serves as an educational tool or toy. A gait of such a robot cannot be performed without foottip slipping with each stride due to its geometry; this results to bigger energy dissipation and more importantly to very inaccurate odometry. On the other hand, Vorpal is a true-omnidirectional vehicle, moreover with possibility of various modifications, e.g., with rotating head turret.

Another class of hexapods are those with 3 DoF per leg. These extends Vorpal-like structure by adding second pitch joint obtaining yaw-pitch-pitch configuration. This enables qualitatively full 3D Cartesian foottip positioning, yet always in two orientations only. Among such robots we mention, e.g., Hexie [26], a novel sibling robot to HAntR, which is focused rather on multi-robot tasks, possibly as remote walking sensor or telecommunication relay beacon. Its overall construction is driven by lowest possible cost, which maintains onboard OrangePi computer allowing for onboard-driven locomotion. However any demanding processing is supposed to be done remotely. It utilises cheaper and smaller Dynamixel XL-320 servomotors, which are on the other hand limiting its payload weight.

PhantomX robot [19] also utilises three DoF per leg. This design is versatile thanks to large area where various add-ons can be placed. AntBot robot [32] has similar construction but is equipped with sensory allowing an accurate localisation by polarised sunlight and simple stride-counting.

Unique mechatronic solution is offered by MorpHex [33], which, having an overactuated body, can fold itself to a sphere and then travel in such pose by means of coordinated raising of individual leg-attached facettes. When unfolded, MorpHex is able to walk like standard 3 DoF hexapod, moreover with variable leg-base diameter. Nonetheless, its design seems space-constrained and does not allow for additional components or surplus computing power.

Using neural networks for control, Lauron V [28] relies on exteroceptive tactile sensing when walking over terrain. The robot, employing 4 DoF per leg in roll-yaw-pitch-pitch configuration, is designed for optimised force and torque distribution, thus its legs are attached unevenly along body. It is also able to manipulate with foreign bodies thanks to *Femur-Tibia Plane* orientation control.

Crabot [27] is an example of importance of compact leg design: Utilising PhantomX Femur and Tibia by flipping Coxa joint and prependeding a new joint resulted to AX-12A servomotors being unable to support robot and stronger servomotors AX-18A had to be used instead.

Fifth degree of freedom allows arbitrary two-axis orientation as seen, e.g., with Weaver [30]. Such a benefit enables better force-control, but at the cost of longer legs with servomotors distributed far from torso. This results in higher leg inertia and thus in worse dynamics.

The main characteristics of the aforementioned robots are summarised in Table 1. We can also mention other robots like Metabot quadruped [34], Hexy the Hexapod [35] or Hexa [36]. Also a quite different approaches to locomotion exist, such as a robot, which can melt its leg and effectively change theirs shape during runtime according to current terrain [37]. But such concept is irrelevant for our purpose because of limited scalability and heating power consumption. Quadrupeds can also serve as an inspiration for hexapod design. MIT Cheetah [13] utilises among other optimisation principles thin leg design, which allow for faster maneuverability and lowers impact forces.

Table 1: Comparison of selected hexapod robots.

Platform	Dof <sup>†</sup>	Size <sup>‡</sup> (L × W × H) [m]	Mass [kg]	Battery capacity [Wh]	Energy density [Wh kg <sup>-1</sup> ]	Operation time <sup>§</sup> [h]	Maximum speed <sup>¶</sup> [m s <sup>-1</sup> ]
X-RHex [21]	6	0.6 × 0.3 × 0.1	9.5	288.0	30.3	3.0	1.54
PhantomX AX [19]	18	0.5 × 0.5 × 0.2	2.6	48.0	18.5	2.0	0.29
Messor II [22]	18	0.5 × 0.5 × 0.2	2.6	cable	-	-	-
DLR Crawler [23]	18	0.5 × 0.5 × 0.2	3.5	cable	-	-	0.20
Snake Monster [24]	18	0.7 × 0.7 × 0.3	4.6	cable	-	-	-
HEBI [25]	18	1.1 × 1.1 × 0.4	21.0	98.0	4.7	>2.0	0.13
Hexie [26]	18	0.2 × 0.2 × 0.1	0.6	18.5	30.5	-	-
Crabot [27]	24	0.7 × 0.7 × 0.3	3.2	28.7	9.0	0.2	0.05
<b>HAntR (Proposed)</b>	<b>24</b>	<b>0.4 × 0.4 × 0.3</b>	<b>2.9</b>	<b>66.6</b>	<b>23.0</b>	<b>&gt;1.0</b>	<b>0.42</b>
Lauron V [28]	24	0.9 × 0.8 × 0.7	42.0	355.2	8.5	>2.0	-
CREX [29]	26	0.8 × 1.0 × 0.2	23.0	177.6	7.7	1.3	0.17
Weaver [30]	30	0.6 × 0.6 × 0.3	7.0	118.4	16.9	-	0.16

<sup>†</sup> Number of controllable DoF.

<sup>‡</sup> Outline of the robot when standing in the default configuration.

<sup>§</sup> Listed values (if known) are reported in the respective cited publications.

## Chapter 2

# List of Design Specifications

The goal of this thesis is to develop a prototype of novel six-legged walking robot platform with 4 DoF per leg. The robot is intended to improve experimental capacity of the ComRob and therefore the design follows a collection of features acquired from five years long experience of the ComRob members, but also from early contemplation about design or ideas inspired by relevant literature. We formulate these features in the following list of Specifications, which we would like to fulfill. A subset of the following list also comprises the thesis assignment.

1. Every robot leg shall be enhanced with the fourth degree of freedom in the yaw-roll-pitch-pitch<sup>5</sup> configuration, which should enable the robot to overcome rougher terrains by extended force-vector control possibilities and better stress distribution between individual joints [18]. We also expect prolonging each leg stride because of possibility to overcome inherent kinematic limitation of the former Femur joint, which disallows leg to reach seamlessly underneath the robot torso. We would consider beneficial if legs would be at least to some degree modular, i.e., that they could be detached and replaced by compatible legs easily. Since each servomotor presents an increased possibility of mechanical failure, we did not want any higher number of actuated joints. Fourth degree of freedom in its own right enables basic manipulation tasks [28], which is not possible with former 3 DoF leg. In combination with possible force-vector control, we expect HAntR will motivate new research on collaborative manipulation.
2. New robot shall have thin foottips improving its locomotion on finer terrains. As the basic controller software presumes the leg is an infinitely thin stick, the former PhantomX legs with foottips c.a. 4 cm wide, was shown to be incompatible with the model. Further, such an excessively wide foottip can causes leg colliding by its side and thus slipping down. Simple controller supposes that even the first imperfect contact was correct and therefore does not compensate for the leg slippage. Furthermore, a path for a cable leading via Tibia, which would allow simple enhancement by sensors attached to leg foottips like tensometers [38] or accelerometers [39] would be favored. We need to enhance foottip with more durable material than the one used on PhantomX but which will maintain adhesion. Former foottips were made of 3 mm thick rubber hose and lasted approximately only three hours of walk until they fretted off. Moreover, their replacement was time consuming. A well-designed Tibia could motivate future controller reckoning with real leg shape or detecting leg beginning to slip.
3. New robot platform shall allow being an omnidirectional vehicle with no preferred direction of travel. Omnidirectionality is a key benefit of a hexapod in comparison to wheeled robots because it enables the robot to move instantly in any direction regardless of the previous configuration, thus making it holonomic. E.g., the PhantomX has two axes of planar symmetry and is also omnidirectional, but it has a preferred direction of travel in longitudinal direction, which inadvertently stresses the middle pair of legs more than the other legs causing them to wear off earlier. We therefore decided to design robot torso with six axes of planar symmetry so identical kinematics, statics, and dynamics are applied among all the legs.

---

<sup>5</sup> Special case of Euler angles (or rather Tait-Bryan angles) in particular representing rotation around former z-axis (yaw), new y-axis(pitch), and resulting x-axes. We represent kinematic structure of orthogonal rotations with it.

## *2. List of Design Specifications*

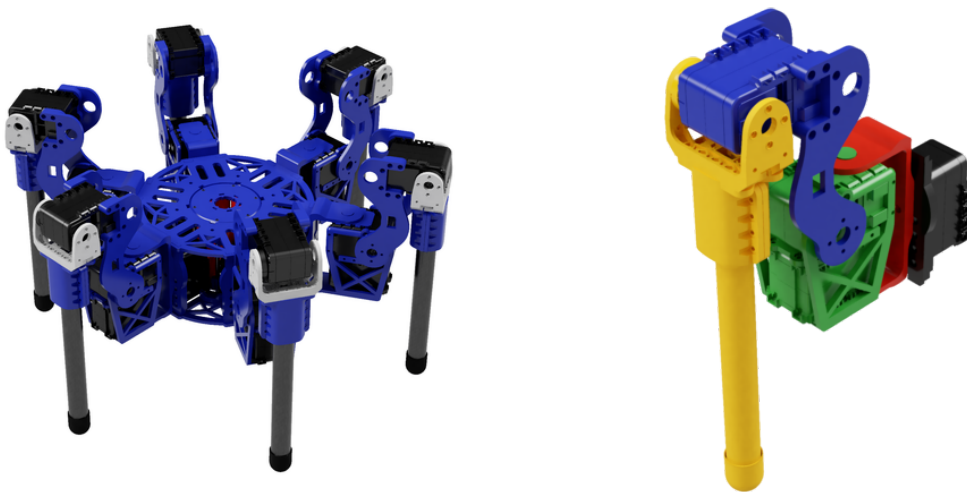
4. The resulting design shall be compact with mass concentrated as close to vertical axis of symmetry as possible. The compact design reduces overall inertia tensor of the robot, and therefore lowers the stress put on the individual servomotors. Thus, we need to place the utilised servomotors as close to torso as possible, leaving the distant parts like Femur and Tibia lightweight. This requirement implies the need for suitable material choice especially for Tibia, which suffers from both continuous and impulsive stress. Further, designing a leg that would allow truly-passive or at least nearly passive pose would allow robot to “sit down” and prolong its operation time. Such a feature could motivate new mission-planning strategies. We can imagine an autonomous robot carrying a communication transceiver, which shall maintain a required position in rough terrain for a prolonged period of time. Moreover, we would like to design the legs in such a way which allows them to fold underneath body and thus making HAntR compact for transportation.
5. It is also required to provide a custom mathematical model of the designed robot comprising of the direct and inverse kinematic tasks. Solving and understanding this will help us to extend this model by Jacobian later on and by adding real physical properties we can obtain dynamic model of the entire robot; but this extension is out of the scope of this thesis.
6. Robot should be able to carry various electronic devices. In the proposed experimental deployments, HAntR is supposed to carry either Odroid XU4 or Nvidia Tegra X2 as the main computer, Intel RealSense D435 together with the XSense MTi-30 attitude and heading reference system (AHRS) as the main sensors, and at least 2600 mA h 11.1 V lithium-based battery. However, we shall design the robot with an appropriate, possibly standardised, mounting mechanism enabling incorporation of electronics with maximum weight of c.a. 1 kg and which fits onto robot torso profile. Our design shall provide a way to wire a multitude of cables through the torso and legs in a way that will not compromise its functionality. Most importantly, we need to manage the paths for cables leading from the torso to the individual legs because such cables are endangered by the leg movements causing the cables to tear apart or crop.
7. Robot shall have enough space for its own reliable and robust power supply of at least three serially connected Lithium-Ion (Li-Ion) type 18650 power cells (each 3.7 V,  $\sim$ 3000 mA h) which together produce 11.1 V, a voltage level that is directly applicable to the utilised AX-12A servomotors. This type of power cells has better properties than the formerly used Lithium-Polymer (Li-Poly) batteries which tended to inflate after several charging cycles and were available in only a few dimensions which constrain the place where they could have been mounted. If we could fit into design any higher number of power cells (connected in parallel), we could increase total energy available for the robot operation, thus improving its endurance. On the other hand, we cannot load too many power cells on the robot because of the limited payload induced by the used AX-12A servomotors. Besides, we shall consider ease of plugging a fresh power source and removing it after use.
8. The robot must have basic software controller and should be aware of its leg positions in order to avoid colliding them together or with the robot body. Such a collision can damage individual mechanical parts and therefore it is required to design a basic leg-leg and leg-body software mechanism to prevent the robot from self-destructive manners.

9. The former PhantomX hexapod torso was manufactured from plastic, which degenerated during the years of service and tended to break during routine tasks. By creating own design, we gain the opportunity to try different materials. In particular, probably those commonly used in the 3D printing like acrylonitrile butadiene styrene (ABS) or polylactic acid (PLA). The goal of this thesis is mainly a proof-of-concept design of a new hexapod platform and further mechanical and material optimisations are left for future work and possible industrial cooperation. Therefore the design being conducted using established and universal tools, which could later serve as reference material, would be considered beneficial.
10. Finally, it is requested to verify the proposed design and developed solution in an experimental deployment. Namely, we shall conduct experiments, which should verify that sloped-terrain balancing was enhanced and that adaptive walking using positional feedback only is possible.

The list of Specifications is hence set up. The desired output of the thesis is to obtain a prototype of the robot with the basic locomotion skills, ready to be equipped with various sensors and computational units. In the next chapter, we describe the proposed solution to meet the list.

## Chapter 3

# Proposed Design



(a) Whole robot rendering. Mechanical parts designed de novo are colored in blue.

(b) Detailed render of a leg with distinguished kinematic links: black–Torso, red–Coxa, green–Trochanter, blue–Femur, yellow–Tibia.

Figure 2: Renderings of the created CAD models.

In this chapter, we provide a thorough discussion of the design process and considerations involved. We have prepared CAD blueprints from which a 3D-printer created a set of parts according to the constraints defined in Sections 3.1.1 and 3.1.2. Considerations regarding utilised CAD software and 3D printing technology are summarised in Section 3.1.3. Those parts assembled with chosen servomotors resulted in the new hexapod robot platform which is ready to be controlled by electronic devices and to perform tasks as slope-balancing and adaptive walking as described in Section 4. Further, based on the mechanical structure, we propose both direct (Section 3.2.1) and inverse (Section 3.2.2) kinematic task solutions utilising the novel 4 DoF leg design; the latter is able to reduce an infinite number of inverse kinematic task solutions to a single one appropriate for Femur and Tibia physical design and also matching assigned orientation. Finally, an overview of basic controller software is presented in Section 3.2.3.

### 3.1 Mechanical Design

We have created an entire new hexapod robot CAD model that is visualised in Figure 2a. The design satisfies constraints implied by the requirements listed in Section 2 and our custom design choices. We have decided to design a leg in the first place and then determine the torso design accordingly. Since

Table 2: List of proposed parts.

Name of part	Pieces used [-]	Weight per part <sup>†</sup> [g]	Section of robot
<i>Servo Facing</i>	6	8.0	
<i>Coxa Bracket</i>	6	12.5	
<i>Trochanter Hoof</i>	6	1.3	
<i>Trochanter Hoop</i> <sup>‡</sup>	6	4.6	
<i>Trochanter Knob</i>	6	2.0	
<i>Femur Clamp</i> <sup>‡</sup>	6	8.0	Leg
<i>Tibia Tube</i>	6	11.5	
<i>Bioloid FP04-F2 Bracket</i>	6	10.6	
<i>Tibia Mount</i>	12	5.7	
<i>Tibia Foottip</i>	6	7.0	
<i>Body Plate</i>	2	28.0	
<i>Battery pack Plate</i>	2	10.0	Torso
Servomotor AX-12A	24	54.6	
Cable 3P	25	3.8	
Cable hubs and convertors	3	5.0	
Odroid-XU4	1	62.0	Electronics
Li-Ion 18650 cell	6	46.8	
Li-Poly battery 2600 mA h	1	190.0	
Xsens MTi-30 AHRS	1	56.0	

<sup>†</sup> An approximate weight; screws, nuts and studs excluded.

<sup>‡</sup> Part has got mirrored Left and Right variants.

the thesis is not focused on mechanical engineering, we felt free to overlarge each stressed component with default thickness of 3 mm. Given Specification 3, all the legs must be identical; hence we design only a single leg, which is manufactured in six pieces. Moreover, because the 3D printing technology is experiencing troubles with arched structures (“overhangs”), we tried to avoid using them in our design. We present a list of used mechanical parts in Table 2 and an isometric drawing of the parts in Figure 3. Drawings of proposed mechanical parts in a defined scale can be found in Appendix A.

Let it be noted that in early stages of the work we hoped that PhantomX robots would only be upgraded with compatible parts or probably whole new legs. We even printed a modified PhantomX torso with a hump big enough for an inflated Li-Poly battery. However, after reading related literature and collecting list of Specifications in Section 2 we have decided to develop an entirely new hexapod robot platform. It was conceptually based on PhantomX design at first, but it changed its shape beyond recognition during the design progress.

### 3.1 Leg

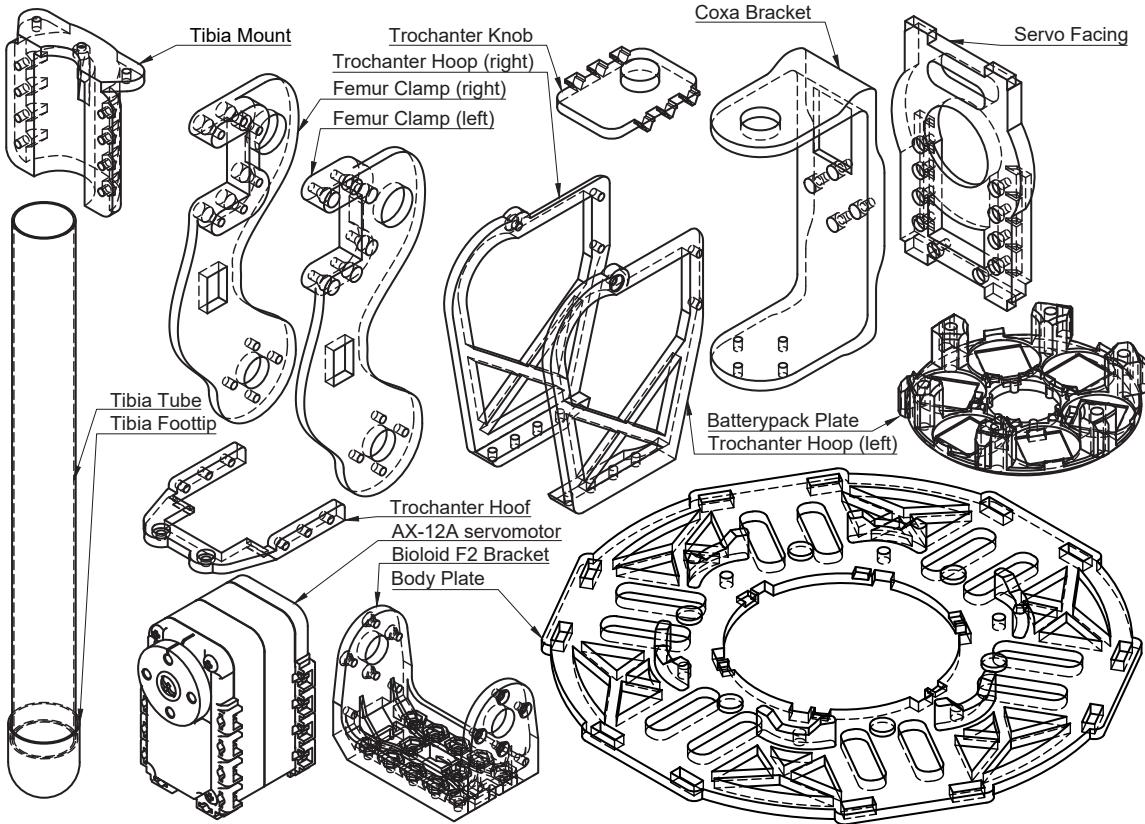


Figure 3: Orthogonal overview drawing of the individual mechanical parts of the robot leg and torso. Connectors like screws, pegs etc. are omitted. Parts are in a relative, further undefined scale. For full technical documentation in a given scale see Appendix A.

#### 3.1.1 Leg

Figure 2b shows the resulting design of the hexapod leg incorporating the fourth degree of freedom required in Specification 1. We have designed the leg in such a way to satisfy the Specification 4 on compact mass distribution while maintaining sufficient reach of the leg and proper cable management. It also utilises brand new Tibia design based on 16 mm carbon fibre tubes, which fully complies with Specification 2. Also, the leg shall have a feasible way of attaching to the robot torso, thus achieving modularity as defined in Specification 1. We shall now describe how we got the design.

First, we must endeavour into simple laws of physics: A force  $\vec{F}$  acting on an object fixed to an axis and outlying by a positional vector  $\vec{l}$  generates torque  $\vec{\tau} = \vec{F} \times \vec{l}$ . In our case, the force is the gravitational force  $\vec{F} = m\vec{g}$  where  $m$  is the object mass, and  $\vec{g}$  is a vector of the gravitational acceleration. We suppose that any leg alternate in two phases only, a support phase and a swing phase. Assuming a quasistatic motion, a leg of any symmetric robot needs to carry a nominal load of one-third of combined torso and swing legs mass during the support phase. In our case, the total weight is approximately 1380 g as apparent from Table 2, therefore each supporting leg is loaded with c.a. 460 g. The support is achieved when a balance of reactive forces and a balance of torques is maintained. A balance of forces is maintained always in each joint unless some excessive force produces strain so large that the mechanical part bends or fractures. A balance of torques can be then either active or passive. We cannot reach a passive torque balance due to required overcomplicated counterweights system. Thus, we must compensate external torques actively by servomotors. Yet, we may try to position the leg so that no torques are present at all. It means placing all leg links along the gravitational vector obtaining  $\vec{l} \parallel \vec{g} \implies \vec{l} \times \vec{g} = \vec{0}$ . During motionless support, this can be achieved

easily even though joints still need to compensate present perturbations; it is a well-known problem of the inverse pendulum—an unstable system. Moreover, the closer the mass is to support points, the less joint-efforts needs to be exerted to keep it in position. This is an incentive for distant mass distribution even though such a condition cannot be met all the time during walk.

On the other hand, during the swing phase, we seek quite the opposite. Any mass weighting  $m$  placed on a radius  $r$  around a rotation axis creates a rotational inertia  $I = m \cdot r$ . If we want to change angular velocity by  $d\omega$ , we need to change its kinetic energy  $dE_k = \frac{1}{2}d\omega^2mr^2$  by exerting torque. We see that energy required for such operation depends quadratically on the radius, and thus if we place mass closer to the axis of rotation, lesser effort needs to be exerted.

With fixed body mass, we see that optimisation for the swing phase is more relevant because support phase problem is only linear with distance. Ideally, we would like to place all those servomotors into one chunk inside torso and from each lead a lightweight mechanism into each joint. Such an approach is being utilised with string-driven joints [40] or pneumatic or hydraulic joint [41]. However, for the sake of simplicity and robustness, we have chosen to attach each servomotor directly to the corresponding link.

Next, we can mention a kinematic principle; when two axes of rotation intersect perpendicularly, the obtained mathematical structure becomes simplified, because respective geometric transformations become a pure rotation.

**Servomotor AX-12A** Since servomotors (in our case Dynamixel AX-12A) are the most massive parts of legs, let us take a closer look at them. Each servomotor has its controller with the integrated P-regulator and is connected via *daisy chain*<sup>6</sup> operated on TTL voltage for the communication and 9–12 V for the power supply. The controller depends on positional feedback implemented by a built-in potentiometer, which cannot cover full 360° angle, and thus leaves a dead angle of 60°. Built-in RAM and FLASH memories storing servomotor configuration and runtime information<sup>7</sup> are directly accessible via Dynamixel 1.0 protocol. Detailed protocol description can be found on web page of the manufacturer [42] or in [43]. Three-wire Dynamixel 3P cables of various lengths are being used to interconnect individual servomotors. Official documentation [44] holds no mention about minimum bending radius, but from our experience we know that cable can be curled down to c.a. 10 mm. These servomotors also offer simple mounting options via M2<sup>8</sup> screws and nuts according to Figure 4b. We can also recon on an already-derived full dynamic model of this motor [46]. When we take into account a limited market with servomotors of similar size with comparable properties, we have no reason to choose different servomotors; larger servomotors are far too powerful and expensive, and the smaller ones would be unable to carry desired loads. Weighting 54.6 g each, servomotors are the most massive part of the proposed leg, thus we need to prioritise theirs positioning towards robot centre. We have considered two main approaches of placing them into the leg morphology.

**The Approach of Extending Former Femur and Tibia** Early contemplation about the leg promised that only upgrading former leg (see Figure 5a) by inserting fourth degree of freedom into various positions could suffice and therefore we could keep PhantomX Femur and Tibia unchanged. Simply prepending a servo next to former Coxa, which would therefore need frontside-back orientation (see Figure 5b), would prolong the leg approximately by 70 mm. Such a design has bad mass distribution which is coincidentally observed with Crabot [27].

<sup>6</sup> Wiring scheme where all involved nodes share a single electrical circuit for communications. This particular implementation uses master/slave protocol for collision avoidance.

<sup>7</sup> Most importantly: ID, an 8-bit number uniquely identifying every servo in single daisy chain; PRESENT\_POSITION and GOAL\_POSITION 10-bit number representing angle between servomotor rotor and its body, mapped to 0° – 300° with 150° as zero-angle; MOVING\_SPEED assigns sets required angular servo velocity in 10-bit number with step of 0.111 rpm.

<sup>8</sup> A particular screw dimension in metric system as defined by International Standard Organisation [45].

### 3.1 The Approach of Redesigning Femur and Tibia

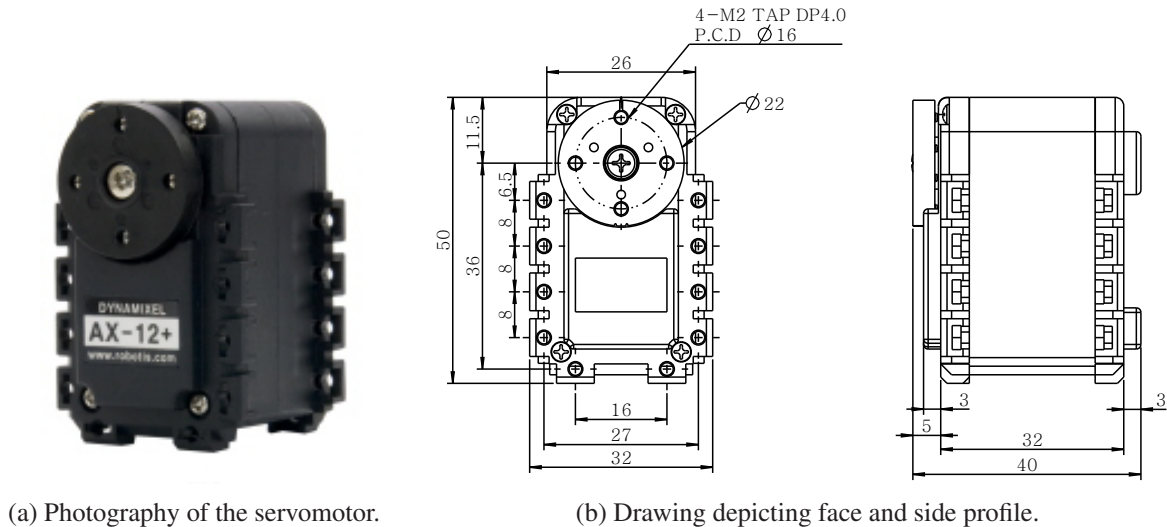


Figure 4: Dynamixel AX-12A servomotor [42].

Other configuration proposed placing first two servomotors one above another similarly to the design of the Weaver hexapod robot (see Figure 5e). This configuration already enhances mass distribution by placing all servos closer to the body. But since such a compound Coxa-Trochanter joint is placed inside robot torso, an additional space is needed for leg to move around its axes; this in turn consumes space which could be otherwise used for electronics. Further, there is an excessive shear force applied on the axis of roll joint, as the leg moments act on it. Weaver robot has metal servomotors with sufficient robustness, but our AX-12A servomotors with plastic gearbox might be damaged by such continuous surplus load.

**The Approach of Redesigning Femur and Tibia** Later, we have also considered leg designs which would solve Specification 2. Every Tibia design allows a passive static pose, but all robots in Section 1.1 allow it only by manipulating legs straight downward. Such a pose is similar to inverse pendulum problem and as known from course on basics of control engineering, the inverse pendulum is unstable. Tibia designed as two parallel clamps (see Figure 5d, similar to Femur link) enables the completely passive pose by folding Femur joint inside Tibia. Walking with such a leg would be possible in the vicinity of such passive pose, moreover with gained stability due to lowered centre of mass. However, this particular design is unfeasible due to Tibia high torsion elasticity. Thus, such a part could not be modelled as a rigid body, and therefore methods proposed in Section 3.2 would not be directly applicable. Further, parallel Tibia would imply either wide foottip or prolonged Tibia both of which we do not desire.

Leg design used in Hexie (shown in Figure 5c) does not allow for entirely passive pose yet nearing it sufficiently. This particular robot is also made from PLA plastic. We had a doubt whether scaled up this part would be strong enough; it is the Tibia which carries all of the assigned weight and suffers from impacts directly, dampening them for other parts. Besides, due to the Hexie Tibia being arched, the manufacturing printing process might not prove appropriate. Lauron V leg (depicted in Figure 5f) cannot be folded in a way similar to Hexie, but shows tubular Tibia design, which incorporates built-in sensory and enables centric mass distribution. However, the Lauron's custom made servomotors are specifically designed to solve the dual-axis Coxa-Trochanter joint, which we cannot replicate using our servomotors.

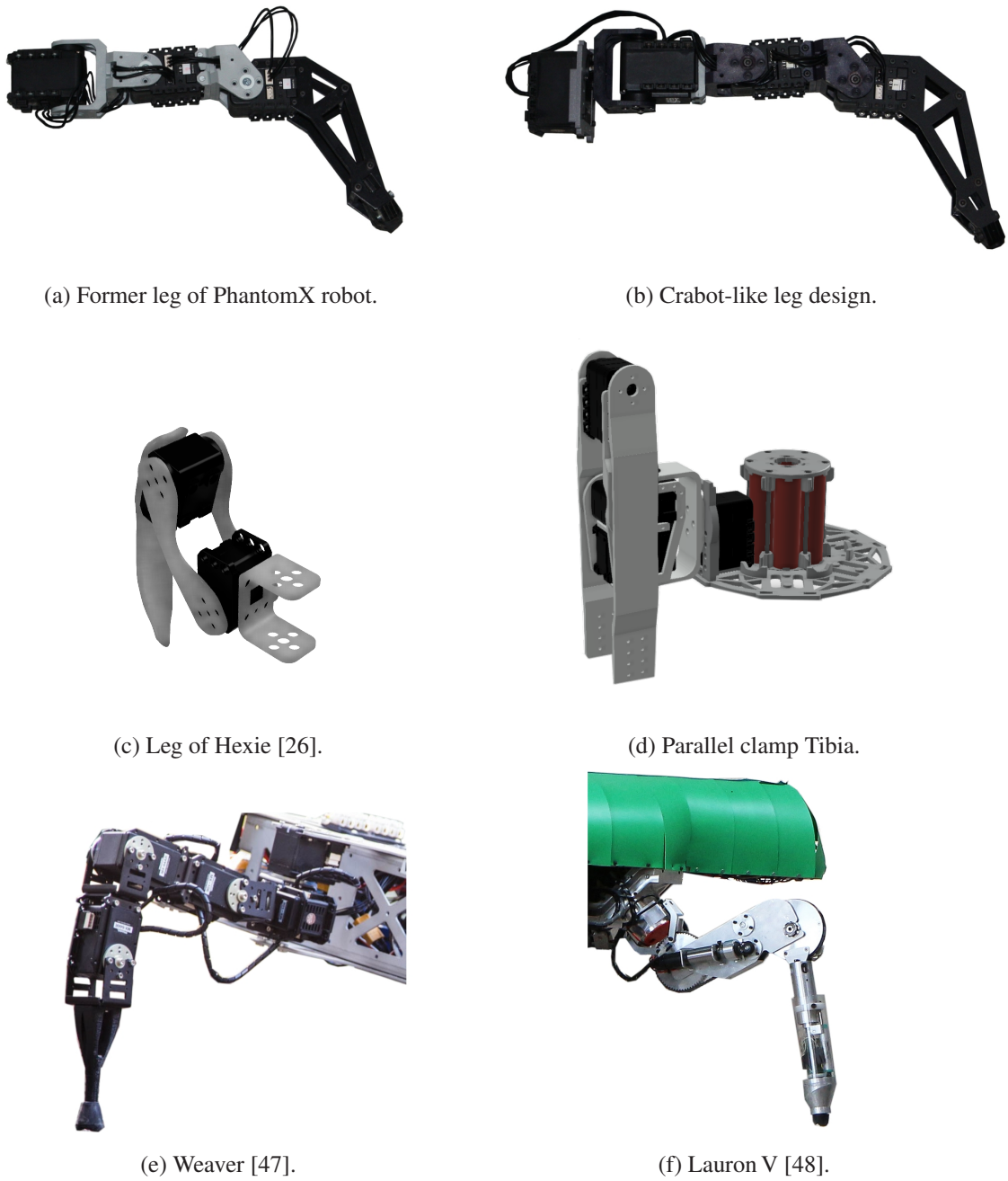


Figure 5: Considered existing leg designs.

### 3.1 Final Solution

**Final Solution** Since given servomotors already constrained us, there is a limited number of possible configurations to consider. Combined with other design constraints, we are left with only a few possibilities to evaluate. Among them, we were able to select the final solution given the following reasoning. It is this particular solution that was later manufactured.

We require to keep future torso compact, which disqualifies Weaver-like Coxa and Trochanter servomotor; the first joint in yaw configuration means that the leg has its lateral operational space too near, hugely overlapping with adjacent leg operating space. Also, it needs more space in the vertical direction making the torso unnecessarily high. But a neat compact design of two servomotors being one above another had also its benefits. So, we decided to place first (Coxa) servo in the roll<sup>9</sup> configuration, followed by *Coxa Bracket* containing no servomotor and allowing for unobstructed motion, as depicted in red in Figure 2b.

Coxa servo is attached to the torso via *Servo Facing*, which helps with the asymmetric load, and which is in turn attached to *Body Plate* via simple lock-in principle: Pegs in *Servo Facing* fit into holes in *Body Plate* which is proven by PhantomX design where miscellaneous electronics are attached likewise. From the kinematic point of view, Coxa servomotor with *Servo Facing* is part of the torso because it is rigidly attached to it, as seen in Figure 2b, black part. We had a possibility to “lay down” servo similarly to Hexie or to even choose some rather different leg. E.g., Lauron V in Figure 5f uses leg based in an angle of 45° from body plane. But we preferred to leave servos “upright” because it reduces the torso diameter and does not leave unused space since the servomotors can be aligned with Batterypack as will be shown later.

Hereafter, we have decided to create compound Trochanter link (green part in Figure 2b) containing actuation for both Trochanter (yaw) and Femur (pitch) joint; therefore the cable connecting these two joints is not threatened by their movement at all. To make the two servomotors rigidly attached, we designed parts *Trochanter Hoof* preventing servomotors from lateral movement, *Trochanter Hoops* holding servos together in the vertical direction, and *Trochanter Knob*, a *Coxa Bracket* counterpart. *Hoof* and *Hoop* were designed to be screwed to AX-12A servomotors, but the *Knob* is meant to only fit freely into its structure, which, when combined with *Coxa Bracket*, prevents it from moving. This whole object is screwed to one side of *Coxa Bracket* and fitted through an opening on the other side.

We have chosen to wire the cable between Coxa and Trochanter servomotors through the upper region of *Servo Facing* because it corresponds to AX-12A inherent dead angle. Unlike different servomotors (e.g., Dynamixel XH-430), AX-12A does not provide a way to wire the cable directly through rotation axis. This path thus induces limitation for achievable angle, as we are unable to reach beyond ±130° without risk of damaging the cable by overstretching it. Further, there is another danger of cutting the cable between *Coxa Bracket* and Trochanter link. This risk is solved by rounding edge of *Trochanter Hoop* and removing material from *Coxa Bracket*. Cable then leads through an opening between Trochanter and Femur servomotors, which was conveniently large enough.

Then, we designed *Femur Clamp* link as two parallel clamps directly attached to the Femur servomotor rotor and Tibia servomotor. The link is also rendered in Figure 2b, particularly in blue colour. The length of this link is the shortest which allows folding Tibia underneath the robot torso. This results in several “compact” poses achievable. *Femur Clamp* is carved by point-fitting spline curve. Pivot points for the splines are chosen to serve two reasons. The first is protecting cable connecting Femur and Tibia servomotors; without them the cable could have been cut between *Femur Clamp* and *Trochanter Hoop* part. The second reason is that we may operate in a near-passive pose with the chosen carving, because the default geometry will have its links less deviated from the gravitational vector. These two reasons motivated our decision to deprecate the design with the parallel Tibias and rather to create a brand-new Tibia as follows.

---

<sup>9</sup> The thesis assignment specified yaw-roll-pitch-pitch configuration instead of roll-yaw-pitch-pitch presented. As we found out, the latter fits better than the former. We believe that our reasoning for this change is sufficient and such a change will be accepted.

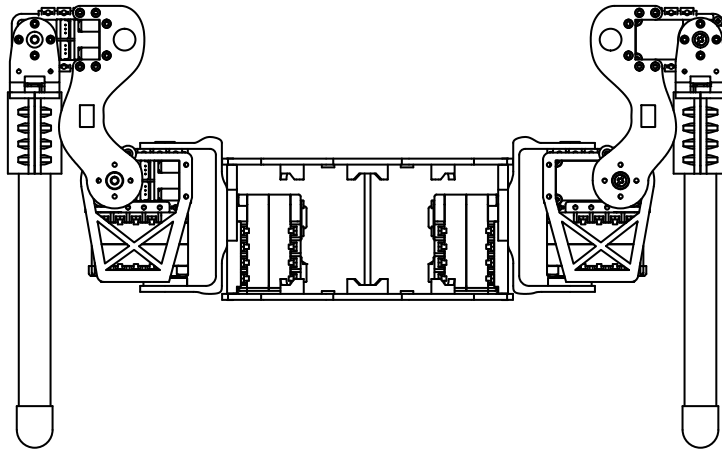


Figure 6: Drawing of the robot torso illustrating how legs are connected to torso and how *Body Plate* desks are held together by studs.

The main part of Tibia link, as depicted in Figure 2b in yellow colour, comprises of *Tibia Tube* made from carbon tube with 16 mm diameter and 0.5 mm thickness. The length of the tube is chosen to be 160 mm making it approximately twice as long as Femur. Besides, the inner diameter allows for future addition of various sensors, similarly to Lauron V. *Tube* is attached to Femur servomotor via standard *Bioloid FP04-F2 Bracket* and *Tibia Mount*. *Tibia Foottip*, which consists of commonly available rubber endings, is located at the other end of *Tibia Tube*. The proposed *Foottip* also offers possibility of fast replacement in case of high wear or when an entirely different shape of the part should be examined, e.g., as seen in [49].

It is worth mentioning, that resulting leg uses primarily M2 screws compatible with the PhantomX. Chosen configuration also improves robustness by negotiating cable joint-crossing. Former PhantomX wired the cables across all three joints. We have improved the cable path so it crosses only two out of four joints, which is also the smallest possible number achievable with 4 DoF open kinematic chain.

### ■ 3.1.2 Torso

Robot torso is composed of two pieces of *Body Plate* held together by three or six studs and shored by six pieces of *Servo Facing* as shown in Figure 6. This setup has been chosen because it allows simple leg-mounting as described earlier and has no overhangs. Along with that, it provides heightened knobs against which Coxa servomotor can lean, thus helping *Servo Facing* with stress resulting from asymmetric load. Placing the servomotors tightly together results in an inside perimeter of 58 mm. There are several holes in the *Body Plate* reducing material required for print; these also serve for attaching Velcro straps, that fix onboard electronics in place.

Resulting leg-placement setup is shown in Figure 7 where we also show how the 18650 Li-Ion cells<sup>10</sup> can fit the interior perimeter. The cells shall be kept in a rigid formation known as Batterypack which is made of two pieces of *Batterypack Plate*. Six cells connected in the 3S-2P configuration<sup>11</sup> and together they provide around 6000 mAh, which is more than the formerly used Li-Poly batteries. The overall capacity can be further extended up to 18 cells (18000 mAh) by adding other triplets of cells into other highlighted positions. On the other hand, such an increased capacity leads to higher mass, and thus care must be taken not to overload individual legs. When no surplus Li-Ion cells are

<sup>10</sup> Cylindrical cell of 18 mm radius and 65 mm height.

<sup>11</sup> A parallel pair of three serially connected cells, producing triple voltage of a single cell and double the capacity.



Figure 7: Rendering of the torso with Coxa servomotors setup and possible Li-Ion cells placement. Green cylinders represent six basic cell positions. Six additional cells can be placed in yellow spots without any troubles—there is enough space for them left. Another six batteries in red spots could be also employed, yet this would demand a major overhaul of torso concept due to collision with *Servo Facing* and possibly even the entire leg.

used, we obtain free spaces which could be later used for miscellaneous small electronics like hubs for servo wiring, interface between USB [50] and AX-12A daisy chain, power convertors or even some additional sensor equipment.

We need to consider also heat dissipation which will be produced by servomotors and batteries. Since we have employed only six pieces of Li-Ion cells in the Batterypack, we believe that heat will dissipate naturally. As an ensuring feature we can add a temperature sensor like PTC thermistor. If heat issues arise, there is always a possibility of attaching an active fan which will blow fresh air around the batteries.

With no additional components, HAntR weights 2.32 kg in the minimal configuration that enables remote control via power and data cable. When equipped for basic autonomous operations (Odroid computer and 2600 mA h Li-Pol battery), weight is around 2.65 kg. It is more than PhantomX whose operational weight can be as low as 2.37 kg. The weight increase is proportional to six new AX-12A servomotors which themselves add roughly 300 g of mass. As further shown in Section 4.3.1, we were able to increase total operation time despite weight increase because of improved mass distribution. We expect HAntR to carry at least 1 kg of arbitrary additional payload, e.g., a transmitter beacon. Since determining the maximal payload by a rigorous method is a time-consuming and complex task, we shall find the maximal payload capacity by computing mass distribution, moments of inertia or performing torque analysis experiment later.

### ■ 3.1.3 CAD Software and Manufacturing Technology

Given the aforementioned constraints, we need to model the most of the passive parts de novo. Let us now, when we already know what to construct, focus briefly on modelling techniques and 3D print technology we have chosen for building the robot prototype, and why we have done so.

**CAD Modeling Software** According to Specification 9, the resulting design is required to be made such that further modifications and mechanical optimisations can be conducted later. It implies utilisation of Computer Aided Design (CAD) software which supports so-called *parametric design*. It is an approach of 3D modelling, where the designer can define some global parameters and reference or adjust some geometry feature properties (e.g., line lengths or angles, distances between bodies) later. From plenty of such software, two of them in particular seems useful for us.

First of them is *OpenSCAD* [51]. It is an open-source programmatic-oriented parametric modelling software based on parsing source files containing geometry definitions; therefrom it creates a corresponding polygonal 3D mesh model of arbitrary resolution that could be altered by setting a minimal allowed angle between neighbouring facets or minimum size of a facet. The geometry is defined by a programming language consisting of basic geometry transformations, such as translation, rotation, intersection, union, scaling, mirroring and few others, and basic 3D bodies creation, e.g., sphere, cube, cylinder and polyhedron. On top of these features, the geometry can be scripted using cycles, variables, functions and inclusions of other source files, which in the total enables complex designs. A benefit uncompetited by the other CAD tool mentioned later is user's full control over design dependencies, model-rendering policies and a possibility to version source files using tools like Git [52] or SVN [53]. However, the main drawback is its terse developing environment lacking some advanced modelling and physical simulation features.

A considered alternative to the OpenSCAD was Autodesk *Fusion360* [54] CAD software, which we tried according to several personal references. This software is a complex tool intended for creating advanced mechanical designs in industry-grade quality with the possibility of automatic generation of blueprints in standardised formats. It features multiple ways of creating a design and then evaluating its mechanical properties by means of numerical simulations of involved physical principles. One particular supported approach is just the mentioned parametric design which we used. Fusion360 implementation of parametric design is through capturing "design history" which is serving a similar purpose to OpenSCAD source files. The resulting CAD model can be portrayed by builtin rendering tool. Sadly, Fusion360 hides all files away from the user to proprietary remote data storage, leaving available only tools which alter them. In comparison to the OpenSCAD, the Fusion360 is cumbersome; sometimes the user is exposed to some unperceivable erroneous behaviour. Such errors may cause some features to lose some references and since the references are inconveniently hidden from the user, they cannot be systematically repaired. Despite such inconveniences, we decided to use Fusion360 because of the overall faster and more agile designing process.

CAD models from either of software tools are obtained in STL file format, that contains resulting mesh model surface geometry as a multitude of elementary spatial triangles. STL file format does not define any additional information about material properties, texture or even length units used. It is only a common agreement that the STL files are generated in millimetre units.

**3D Print Technology and Related Material Choices** We manufactured resulting design using currently already mature and widely available method of additive layered 3D printing from plastic material because of its simplicity, relative speed of process, and yet mechanically sufficient properties of resulting objects. It is a method of automated plastic wire (*filament*) melting and extruding in a thin layer onto a printer bed or previous layer in the precise position. The physical properties of the used plastics ensure that the previous layer gets melted by a heat of the new layer. Partial diffusion then binds them solidly together. It is the low temperature of melting<sup>12</sup> that makes this technology so useful and safe even for public usage. However, the basic technology cannot create a flawless merging of layers, which results in strong anisotropic properties. E.g., this resulted to our choice of printing *Coxa Bracket* such that the "stronger" direction was aligned with main stress direction.

---

<sup>12</sup> E.g., PLA plastic softens at temperatures around 60 ° C and melts completely at c.a. 180 ° C. Since such materials are amorphous they have no precise melting temperature.

There are several materials, that can be used in this technology like ABS, PLA, and others ranging from plastic-wood combinations to titanium laser-sintering technology; the former two are well available for public usage. The ABS plastic has slightly better mechanical properties but at a cost of more difficult printing process mainly because of significant thermal deformation due to heterogeneous heating. It also requires higher temperatures and produces toxic gases which should be properly ventilated. On the other hand, printing from PLA has got these drawbacks in much smaller measure. It should sustain stress comparable to the ABS and since it has a much simpler printing process, we have chosen to print all parts from PLA plastic on the Prusa i3 Mk3 printer. More on 3D printing topic can be found in, e.g., [55].

Before the actual 3D printing, CAD models obtained from modelling software as a STL file must be processed by a “slicer” software first. The slicer divides required rigid body into horizontal layers and in each layer it finds a path and instructions for the printer extruder, which prints the object.

After finishing the print, a real-world verification of resulting items needed to be made. It has been shown that when we need two mechanical parts to fit tightly together as, e.g., *Body Plate* and *Servo Facing*, we had to make a gap of 0.15 mm between any two faces of the bodies. Besides, we were sometimes forced to modify already printed material with common tools like shears, pliers or box cutter. We encountered only a handful of problems which required posterior care and we fixed all of them in later versions of individual parts. Yet only a single thing is left for after-print work: *Servo Facing* and *Coxa Bracket* adjacent faces has to be brushed with very fine (P 2000) sandpaper to reduce their friction.

Tibia Tube which is not printed has been made from carbon tube which is being sold in 1 m length. We used Dremel-3000 micro router with attached iron-cutting disk to cut the tube. Since we had no proper support, resulting cut was jawed and thus imprecise. During cutting, we strongly recommend using some mask for breathing and ideally pour water over tube during cutting to avoid health risks caused by fine carbon-epoxy dust.

## 3.2 Kinematics and Control

In the previous section, we discussed and reasoned mechanical properties of HAntR. Now we need to describe resulting physical object by mathematical tools which will enable us to control it. Let us first introduce a numbering of the objects involved as depicted in Figure 8 to systematically address the following description. Each of HAntR legs has its unique number  $l \in \{0, 1, \dots, 5\}$ . Each leg consists of four joints and four links. Each joint and related link shall have assigned number  $j \in \{0, 1, 2, 3\}$ . Simple calculations create a mapping of  $(l, j) \leftrightarrow i$  as

$$i = 4l + j, \quad l = \frac{i}{4}, \quad j = i \bmod 4, \quad (1)$$

where  $i$  is directly used as the AX-12A servomotor ID.

In the following text, we shall derive the direct kinematic task (DKT) and the inverse kinematic task (IKT). These tasks provide a very important mathematical mapping between the joint space  $\mathcal{Q}$  and the robot-related Euclidean space  $\mathcal{C}$ . Let us define fundamental terms and assumptions for proper problem description first.

- ${}^k_l \mathcal{T}_B^A$  represents an Affine (homogeneous) transformation from a reference frame  $A$  to a reference frame  $B$  with possible descriptive indices  $k$  and  $l$ . By reference frame, we mean an oriented origin, a point with three orthonormal unit vectors. We can also contextually refer to such reference frame as to its null vector.
- We access an  $i^{\text{th}}$  element of an object  $O$  by notation  $O_i$ . The index can be both numeral and literal, e.g.,  $O_3$  or  $O_x$ .

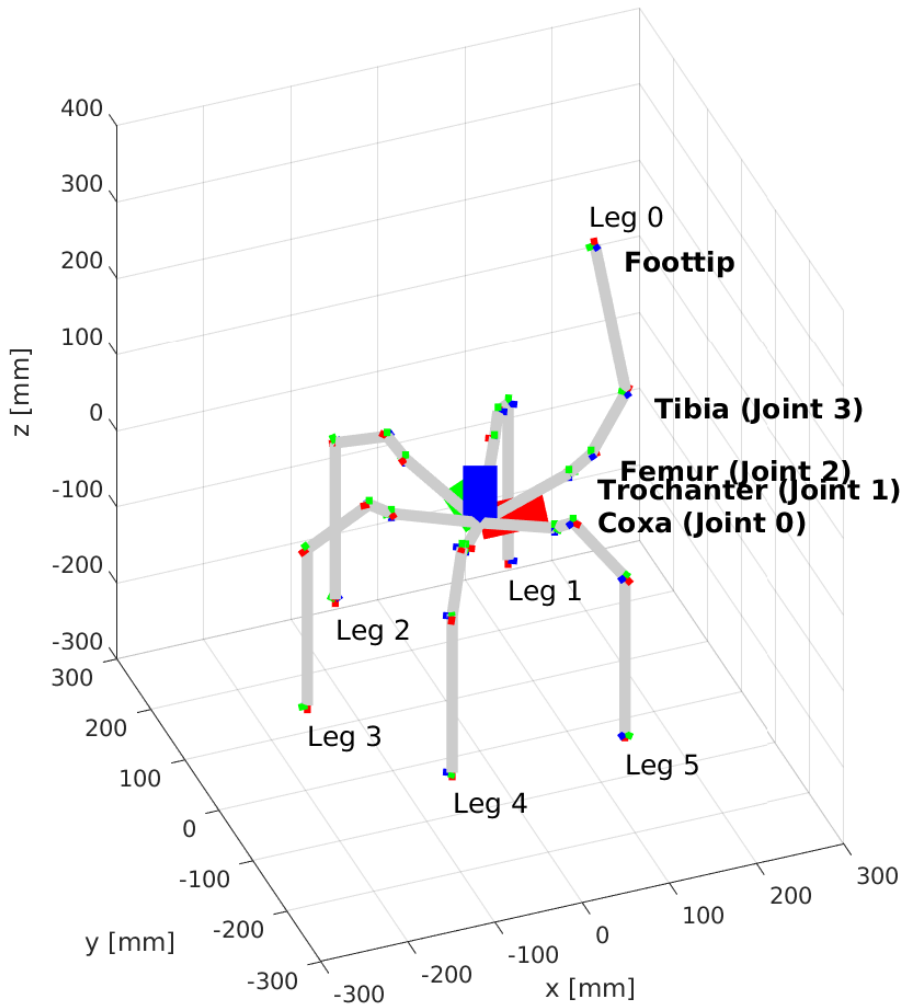


Figure 8: Visualisation of a multi-legged robot mathematical model. We can see the the reference frame of HAntR, individual legs, and foottips.

### 3.2 Direct Kinematic Task

- HAntR exists in a *global environment* (real world), which can be locally idealised as a 3D Euclidean space  $\Gamma$  with Cartesian coordinate system of the origin  $\Gamma_0$ .
- HAntR has its Euclidean space  $\mathcal{R}$  being affine subspace of  $\Gamma$  with the origin  $\mathcal{R}_0$  attached and aligned to its torso as depicted in Figure 8. Torso has got 6 DoF since it well corresponds to the rigid body model.  ${}^p\mathcal{T}_{\mathcal{R}_0}^{\Gamma_0}$  is a transform representing position of and orientation HAntR w.r.t.  $\Gamma$ .
- Each of HAntR links also has its attached affine space with a reference frame. For given leg, we can name those reference frames as  $J_0, J_1, J_2, J_3$ , where  $J_0$  is also a reference frame of the entire leg, and  $J_4$ , denoted also as  $E$ , for the foottip-attached reference frame.
- HAntR has got 24 joints in total, each of them has got 1 DoF in its own right. The robot torso has got 6 DoF, because it is a rigid body. Altogether, an object of 30 DoF is obtained.
- $\mathcal{Q} = \mathbb{R}^{24}$  is a set of all possible joint-coordinates with  $i^{\text{th}}$  value corresponding to the  $i^{\text{th}}$  servomotor or joint.  $\hat{q} \in \mathcal{Q}$  is a vector enumerating particular joint configuration.  $Q = \mathbb{R}^4$  is a set of all possible joint-coordinates for a single leg.  $\vec{q} \in Q$ ,  $\vec{q} = (\hat{q}_{4l}, \hat{q}_{4l+1}, \hat{q}_{4l+2}, \hat{q}_{4l+3})$  is a vector enumerating particular configuration of the leg  $l$ .
- Similarly,  $\mathcal{C} = \mathbb{R}^{18}$  is a set of all foottips.  $\hat{c} \in \mathcal{C}$  is a vector enumerating particular foottip position configuration.  $C = \mathbb{R}^3$  is a set of all possible foottip positions for a single leg.  $\vec{c} \in C$ ,  $\vec{c} = (\hat{c}_{3l}, \hat{c}_{3l+1}, \hat{c}_{3l+2})$  is a vector enumerating particular foottip position of the leg  $l$ . Let us explicitly emphasise that these  $\hat{c}$  and  $c$  describe solely foottip position, not orientation.

#### 3.2.1 Direct Kinematic Task (DKT)

We can define leg-DKT for a leg  $l$  with the given joint coordinates  $\vec{q}$  as a mathematical mapping  $Q \rightarrow C$ , which corresponds to  $\mathbb{R}^4 \rightarrow \mathbb{R}^3$ . Such mapping always yields a single solution because it utilises nothing else than linear transforms based on regular matrices yielding a single solution by definition. The mapping is not surjective since it cannot reach every point; inner unreachable space emerges due to uneven lengths of Femur and Tibia links, outer unreachable space emerges due to finite lengths of Femur and Tibia. Neither it is injective; there are multiple possible joint configurations which reach a single Cartesian position. E.g., when  $E$  lies on leg  $x$ -axis, we can get an infinite number of possible joint configurations reaching the same Cartesian point by choosing arbitrary  $q_0$ .

Since every leg forms an open kinematic chain, we can utilise proven techniques of analysis [15]: We can define *static transformation*  ${}^S\mathcal{T}_{J_0}^{\mathcal{R}_0}$  first, that can be constructed as

$${}^S\mathcal{T}_{J_0}^{\mathcal{R}_0} = \mathfrak{R}(z, l60^\circ) \mathfrak{V}(102, 0, 38.5) \mathfrak{R}(y, 90^\circ) \mathfrak{R}(z, 90^\circ), \quad (2)$$

where  $\mathfrak{R}$  stands for an elementary rotation  $\mathfrak{R}(\text{axis, angle})$  and  $\mathfrak{V}$  is a translation  $\mathfrak{V}(x, y, z)$ . The particular values have been read from Fusion360 drawings and verified using a caliper. Resulting  $J_0$  origin lies in Coxa and Trochanter rotation axes intersection and its  $z$ -axis is aligned with the axis of rotation of Coxa servomotor.

The static transform allows us to employ Denavit-Hartenberg (D-H) notation [15], an apparatus devised for describing general open kinematic chain as a series of homogeneous transformations, one per each joint in the analysed kinematic chain. The concept is extended by making this matrix a function of joint coordinates  $\vec{q}$ . For the joint  $j$  with the joint coordinate  $\vec{q}_j$  the D-H transformation

Table 3: Denavit-Hartenberg parameters table describing geometry of each leg.

Joint name	$j$	$\theta_j$ [°]	$d_j$ [mm]	$x_j$ [mm]	$\alpha_j$ [°]
Coxa	0	0	0	0	90
Trochanter	1	90	-18.5	25.4	-90
Femur	2	-29.5	0	81.6	0
Tibia	3	-60.5	0	205.5	0

matrix  ${}^j\mathcal{T}_{j+1}^j(\vec{q}_j)$  with parameters  $\theta_j, \alpha_j, x_j$  and  $d_j$  can be defined as

$${}^j\mathcal{T}_{j+1}^j(\vec{q}_j) = \begin{bmatrix} \cos(\theta_j + \vec{q}_j) & -\sin(\theta_j + \vec{q}_j) \cos(\alpha_j) & \sin(\theta_j + \vec{q}_j) \sin(\alpha_j) & r \cos(\theta_j + \vec{q}_j) \\ \sin(\theta_j + \vec{q}_j) & \cos(\theta_j + \vec{q}_j) \cos(\alpha_j) & -\cos(\theta_j + \vec{q}_j) \sin(\alpha_j) & r \sin(\theta_j + \vec{q}_j) \\ 0 & \sin(\alpha_j) & \cos(\alpha_j) & d_j \\ 0 & 0 & 0 & 1 \end{bmatrix}. \quad (3)$$

The four parameters  $\theta_j, \alpha_j, x_j, d_j$  completely describe the geometry of each joint and its attached link. Individual parameters denote transformations;  $\theta_j$  defines an offset of rotation around the former  $z$ -axis,  $d_j$  is a translation along the former  $z$ -axis,  $x_j$  is a translation along the resulting  $x$ -axis and  $\alpha_j$  is a rotation around the resulting  $x$ -axis. HAnR employs only revolute joints; thus parameter  $d_j$  is always a static parameter, never a variable-offset as seen with prismatic joints. The values for these parameters were obtained from Fusion360 drawings and then verified by physical measurements with a caliper and are summarised in Table 3. Thanks to perpendicular intersection of Coxa and Trochanter servomotor rotation axes, Coxa row of Table 3 holds only a single entry, making it simpler than if it was otherwise.

We receive compound homogeneous transformation with the arbitrary number  $j' \in \{0, 1, 2, 3\}$  by appending individual D-H transformation matrices after  ${}^S\mathcal{T}_{J_0}^{R_0}$ .

$${}^D\mathcal{T}_{J_{j'}}^{R_0}(\vec{q}, j') = {}^S\mathcal{T}_{J_0}^{R_0} \prod_{j=0}^{j'} {}^j\mathcal{T}_{j+1}^j(\vec{q}_j). \quad (4)$$

Finally, we obtain the solution of DKT by projecting zero vector with the last transformation matrix as

$$[\vec{c} \ 1]^T = {}^D\mathcal{T}_E^{R_0}(\vec{q}, 3) [0 \ 0 \ 0 \ 1]^T. \quad (5)$$

It is worth noting that we can limit the number of joints considered in DKT by choosing different value of  $j'$  and therefore we can compute coordinates of any link or even leg base for  $j' = 0$ . This feature is utilised in the solution of the inverse kinematic task.

Computing a DKT for the whole  $\hat{q}$  is done by executing leg-DKT for different  $l$  and simply composing final vector. We are aware that this mathematical model will differ from reality because of imperfect manufacturing and random fluctuations. It could be negotiated e.g. by careful calibration. The DKT computation can be further extended by computation of positions and orientations of centres of masses of each of 25 rigid bodies from which HAnR is composed. It supports a solution of so-called direct dynamic task which can, in turn, enable us to simulate the robot movements. We consider such an extension to be out of the scope of this thesis.

### 3.2 Inverse Kinematic Task

#### 3.2.2 Inverse Kinematic Task (IKT)

Now we want to define the opposite computation. We want to obtain joint coordinates which correspond to a given Cartesian coordinates. We already saw, that if there exists a solution at all, then there exists an infinite number of other feasible solutions. Thus, we need to reduce the of solutions.

We can fix joint 1 or joint 2 with an arbitrary value and effectively reduce the task to problem already solved with 3 DoF robots. But we rather introduced an *ideal footprint orientation constraint*  $\vec{o}$  which is of same algebraic topology as  $\vec{c}$ . It represents a free Cartesian vector w.r.t. origin of the body reference frame, which defines an oriented line along which we try to align  $E$  as best as we can. Thanks to non-linear character of underlying equations, applied vector  $\vec{o}$  does not overs constrain the task, but leaves us with several solutions. Instead of pure algebraic approach, we chose to perform careful problem analysis, identify spots where the number of solutions multiplicate and tackle them.

We begin our analysis by observing leg behaviour. Femur and Tibia joints have their axes of rotation parallel; thus respective links lie in the same plane and by proper actuation, they allow positioning in both dimensions of that plane. Let us call this plane *Femur-Tibia Plane* or shortly *FTP*. We define this plane by point  $J_0$  and its normal vector  $\vec{n}^{FTP}$ , both w.r.t.  $\mathcal{R}_0$ . Also, we can see that configuration of the entire FTP is determined solely by joints Coxa and Trochanter; therefore we can decouple the leg-IKT computation into two steps:

**Coxa and Trochanter** The computation for the leg  $l$  with given vectors  $\vec{c}$  and  $\vec{o}$  (both w.r.t.  $\mathcal{R}_0$ ) begins by computing static transformation  ${}^S\mathcal{T}_{J_0}^{\mathcal{R}_0} = {}^D\mathcal{T}_{J_0}^{\mathcal{R}_0}(\emptyset, 0)$ , yielding the reference frame origin  $J_0$  w.r.t.  $\mathcal{R}_0$ . We then apply the additional input of  $\vec{o}$  to compute the desired FTP normal vector as

$$\vec{n}^{FTP} = \frac{\overrightarrow{J_0E} \times \vec{o}}{|\overrightarrow{J_0E} \times \vec{o}|}. \quad (6)$$

With this step we introduced a potential computational singularity when  $\vec{n}^{FTP}$  gets close to being parallel with  $\overrightarrow{J_0E}$ . In such a case fatal numerical inaccuracies may arise; therefore we must restrict operations of HAntR, so this situation does not happen.

Inconviniently, because of right-hand rule, we can get different orientation of resulting  $\vec{n}^{FTP}$  when  $c$  and  $o$  “flips” their positions. As it is going to be presented be seen later, this would impose a danger when computing with  $\arcsin$ . We therefore modify  $\vec{n}^{FTP}$  as

$$\vec{n}'^{FTP} = \begin{cases} -\vec{n}^{FTP} & : \vec{n}_x^{FTP} < 0, \\ +\vec{n}^{FTP} & : \text{else.} \end{cases} \quad (7)$$

The  $\vec{n}'^{FTP}$  specifies an *axis of ideal orientation* which is now directionless. Combined with point  $J_0$  we obtain desired FTP configuration. We need to know how shall we set Coxa and Trochanter to achieve the configuration.

By solving a set of linear equations, we express vector  $\vec{n}''^{FTP}$  w.r.t.  $J_0$  obtaining  $\vec{n}'''^{FTP}$  as

$${}^S\mathcal{T}_{J_0}^{\mathcal{R}_0} \vec{n}'''^{FTP T} = \vec{n}'^{FTP T}. \quad (8)$$

Now, we can employ another observation that when zero joint coordinates are projected through DKT,  $\vec{n}'''^{FTP}$  is identical to  $J_0$   $x$ -axis. Also, we see from the Table 3 that these joints represent two rotations

$$\mathcal{T}_{J_2}^{J_0} = \mathcal{R}(\vec{z}, \vec{q}_0) \mathcal{R}(\vec{y}, \vec{q}_1). \quad (9)$$

If we project  $J_0$   $x$ -axis through  $\mathcal{T}_{J_2}^{J_0}$  and compare to  $\vec{n}^{FTP}$  we obtain a set of nonlinear equations

$$\begin{aligned} \cos(\vec{q}_0) \cos(\vec{q}_1) &= \vec{n}''_x^{FTP}, \\ \cos(\vec{q}_1) \sin(\vec{q}_0) &= \vec{n}''_y^{FTP}, \\ -\sin(\vec{q}_1) &= \vec{n}''_z^{FTP}. \end{aligned} \quad (10)$$

Equation 10 can be solved directly using by cyclometric functions as

$$\begin{aligned}\vec{q}_0 &= \arctan(\vec{n}''_y^{FTP}, \vec{n}''_x^{FTP}), \\ \vec{q}_1 &= \arcsin(\vec{n}''_z^{FTP}),\end{aligned}\quad (11)$$

where  $\arctan$  means four-quadrant oriented version of the function. This is the primary solution for joint coordinates  $q_0$  and  $q_1$ .

The cyclometric functions are defined only in a limited range, but due to respective goniometric function being non-injective, other solution can be obtained as  $\vec{q}'_0 = \vec{q}_0 + \frac{\pi}{2}$  and  $\vec{q}'_1 = -\vec{q}_1$ . As we will see in Table 4 the other solution would never be physically feasible, so we discard it straightaway. We can also see now, that if we omit Equation 7, the  $\arcsin$  function could have shown discontinuous behavior when  $z$ -axis changes its value between  $-1$  and  $1$  rapidly which is possible when  $\vec{o}$  and  $\vec{c}$  moves through collinear state.

Despite having solved discontinuity of  $\arcsin$ , we still cannot get smooth movement, because with fixed  $\vec{o}$ ,  $\vec{c}$  can pass  $J_0$   $xy$ -plane in a single point only. To perform smooth movement across mentioned  $xy$ -plane, we need to extend IKT further, maybe with some motion-planning algorithm. Or we could simultaneously compute another IKT with convenient  $\vec{o}$  which would enable seamless discontinuity cross and merge these two results by, e.g., weighted average according to the Euclidean distance to the discontinuity. However, these methods are not in the scope of this thesis and need further research and validation. For now, we shall limit reachable Cartesian space to  $J_0$   $z$ -axis-positive side.

**Femur and Tibia Solution** Now we can focus on computing the rest of joint coordinates. Since we already derived both  $\vec{q}_0$  and  $\vec{q}_1$ , we may compute transformation to Femur origin  $\vec{J}_2$  as a partial DKT. Such a transform enables us to express  $\vec{c}$  w.r.t.  $J_2$  as  $\vec{c}'$  via another solution of the system of linear equations as

$${}^D\mathcal{T}_{J_2}^{\mathcal{R}_0}([\vec{q}_0, \vec{q}_1, 0, 0], 2)\vec{c}' = \vec{c}. \quad (12)$$

Let us now consider a planar task in FTP which equals to  $J_2$   $xy$ -plane. We utilise our knowledge about movement constraints of Femur and Tibia links. Tibia is fixed by one end to  $c'$  as well as Femur is fixed by one point to  $J_2$ . Therefore their other ends may be found on circles around null vector (which is a Femur origin) and  $c'$  (which is footprint position) with respective radii  $f, t$  equaling to link lengths as in Table 3. Their other ends are also coincident; thus we can find Tibia origin by computing the Planar Circle Intersection Task.

In such a task, we have two arbitrary points  $A$  and  $B$  (in our case a null vector and  $c'$  respectively) and two radii  $a$  and  $b$  (in our case  $f$  and  $t$ ). We find out whether the circles intersect at all by a simple comparison between distance  $d = |A - B|$ : If  $d \geq a + b$ , we say that centres of circles are too far away to intersect or they intersect in a single point which is a singular case which we shall neglect by forbidding such cases. When  $d \leq |a - b|$  we say that centres of circles are too close to each other to intersect or they intersect in a single point which we shall neglect as well. If none of those conditions is met, we conclude that circles intersect as two points symmetrically placed around abscissa  $\overleftrightarrow{AB}$ , as shown in Figure 9.

We can express Pythagorean equations of both  $\triangle ASX_1$  and  $\triangle BSX_1$ . Using  $n = d - m$  with the proper treatment we obtain

$$\begin{aligned}v^2 &= a^2 + m^2 = b^2 + n^2, \\ b^2 - a^2 &= m^2 - n^2 = (m - n)(m + n) = (2m - d)d, \\ m &= \frac{a^2 - b^2}{2d} + \frac{d}{2}.\end{aligned}\quad (13)$$

### 3.2 Femur and Tibia Solution

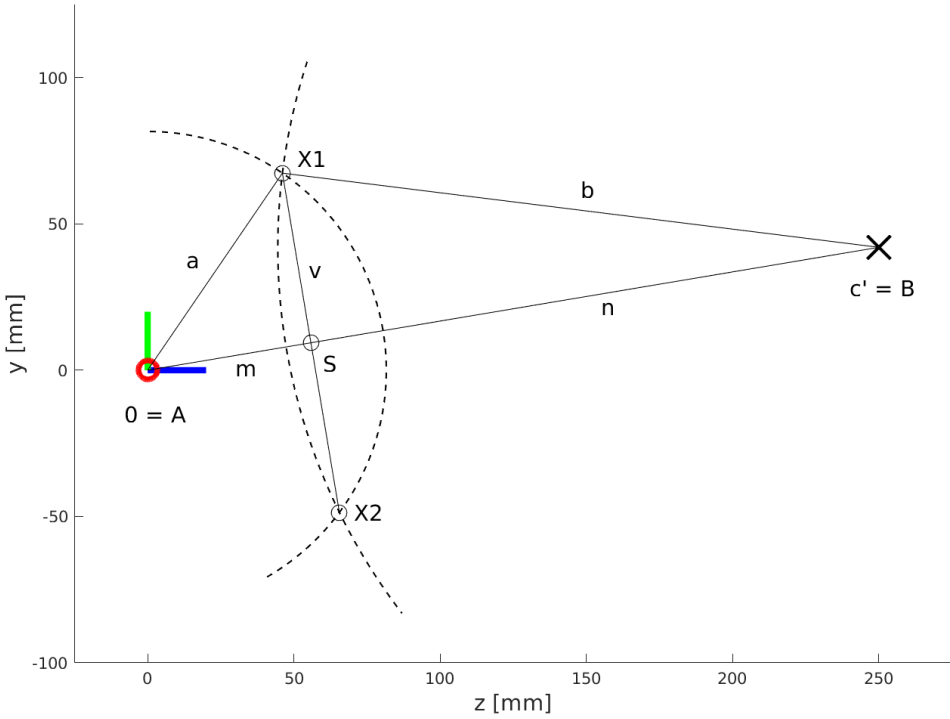


Figure 9: Situation in FTP – circle intersection problem.

From  $m$  we can compute the point  $S$  as

$$S = A + m \frac{\overrightarrow{AB}}{d} \quad (14)$$

and distance  $v$  as

$$v = \sqrt{a^2 - m^2}. \quad (15)$$

The intersection points  $X_1$  and  $X_2$  are then computed using 2D rotation  $\mathcal{R}(q)$  as

$$X_{1,2} = S \pm \mathcal{R}_2(90^\circ) \vec{v} \frac{\overrightarrow{AB}}{d}. \quad (16)$$

These two solutions can be further reduced to a single one; since Femur and Tibia are designed to be concave in the FTP, we can enjoy the liberty of choosing  $X_1$  as the “upper” point as

$$X = S + \mathcal{R}_2(90^\circ) \vec{v} \frac{\overrightarrow{AB}}{d}, \quad (17)$$

thus always achieving concavity as designed.

Computing  $q_2$  and  $q_3$  remains. We need to know theta-offsets of Femur and Tibia joints  $\theta_2$  and  $\theta_3$  from Table 3. We stay in FTP and according to our observations we set that

$$\vec{q}_2 = \arctan(X_y, X_x) - \theta_2, \quad (18)$$

$$\vec{q}_3 = \arctan((\vec{c}' - X)_y, (\vec{c}' - X)_x) - \vec{q}_2 - \theta_2 - \theta_3. \quad (19)$$

Now we know all the joint coordinates. Moreover, we always get a single meaningful solution despite IKT being non-linear task potentially yielding infinite number of solutions.

Table 4: Fixed joint coordinates safety limits.

Joint name	$j$	$q_j^{\min}$ [°]	$q_j^{\max}$ [°]
Coxa	0	-135	135
Trochanter	1	-90	90
Femur	2	-90	135
Tibia	3	-45	90

We can further extend the IKT solution by a self-collision detector. The most straightforward way to prevent a leg from interfering with itself, with other legs, or other bodies is by introducing carefully chosen fixed limits for joint angles. In case of HAntR such limits are presented in Table 4.

Since every floating-point computation on nowadays machines may contain errors [56], comparing arbitrary two numbers can seldom result in a match. We need to compare numbers approximately with an  $\epsilon$  of value around  $10^{-5}$  to obtain meaningful results.

Hereby, we derived both direct and inverse kinematic tasks. The DKT always yields only a single solution for any given joint coordinates. Now it is useful for purely kinematic and geometric applications but it can be easily extended for dynamics-related tasks. IKT is also solved with always-single solution despite being a complex nonlinear task. Also, important numerical and geometrical singularities are treated, so they impose no danger during runtime. It is important that when we set  $q_0 = 0$  or when we set  $\vec{o} = [0, 0, -1]$ , we obtain the same 3 DoF configuration as with the former PhantomX robot. This is vital for future examination of fourth DoF benefits. The control of the robot limbs is thus enabled, and we may proceed with developing basic gaits.

### 3.2.3 Implementation

An implementation of both IKT and DKT has been made in C++. It can be deployed on various computational platforms such as personal computers, embedded Odroid-XU4, or even on microcontrollers like STM32 Nucleo or Arduino. We created a Hexapod class that can be reused by another program, e.g., programs executing individual experiments described in the following part. The controller uses Eigen library offering implementations of various Linear Algebra problems. Most importantly, we use generic solvers of systems of linear equations, particularly *Householder algorithm of QR decomposition with column pivoting*.

The per-leg kinematic tasks can be accessed by methods `leg_DKT` and `leg_IKT`, with method `leg_reachable` implementing joint limits introduced in Table 4. Leg-wide or body-wide servomotor read and write operations can be performed with `HAL_leg_read`, `HAL_leg_write` and `HAL_RW_J` respectively, the latter also offering a utility of logging desired and current joint coordinates. Function `HAL_readTemperature` scans all the servomotors and extracts information about current temperature. These utilities use existing Bioloid controller [57] as a form of Hardware Abstraction Layer. Utility functions `pose_sit` and `pose_home` commands the servomotors, forcing the robot into predefined configurations with no further control.

The current implementation can perform both read and write operations at c.a. 2 ms per servomotor resulting in 48 ms for all 24 servos, the kinematics computations lasting less than 1 ms. Despite this, we rounded the control loop period to 50 ms to get a safety margin in case of unexpectedly prolonged computations on the non-realtime operating system. In the future, control loop can be enhanced by Sync Write and Bulk Read packets or by [43].

# Chapter 4

## Verification

After finishing the design process by deriving and implementing the kinematic tasks, we had the last step ahead. We had to examine the resulting properties of the developed platform. In the beginning of this chapter in Section 4.1 we discuss the resulting mechanical properties with included list of known mechanical issues. Then an IKT proof-of-concept is shown in Section 4.1.1; knowing that task is solved correctly, we may proceed with other experiments. In Section 4.2 we discuss the adaptive locomotion gait using servomotor positional feedback only [16, 46] using a constant-threshold method. First, we had to derive the static threshold by examining characteristics of regulating error signal during footstrike which is described in Section 4.2.1. Therefrom we were able to implement a seamless tripod gait controller and measure whether enabled footstrike detection lowers vibrations on HAntR. Finally, we conducted experiments inspecting endurance (Section 4.3.1), approximate maximum locomotion speed test (Section 4.3.2), and ability of slope-balancing of HAntR (Section 4.3.3).

We used an Apriltag visual measurement system [58] for experiment evaluation. The measured robot had to be furnished with a marker, second marker was then fixed to the ground. The whole scene was continuously monitored by a calibrated camera (e.g., see Figure 21a) and later processed on computer. Thanks to prior information about marker size, we obtained a timestamped log of positions of the individual markers present, each in terms of homogeneous transformation matrices w.r.t. camera reference frame. Thus, we were able to express the position and orientation of the robot-attached marker w.r.t. the grounded marker by solving a system of linear equations. According to information provided by authors, this method offers neglectable inaccuracy at distances below 20 m; in indoor, the distance was indeed complementary.

Also, we utilised logging function proposed in Section 3.2.3. The joint-coordinate data was available at control loop frequency of 50 Hz as opposed to the temperature data, which was gathered each time a stride-interpolating loop finished. After careful evaluation, it was shown, that the current prototype of HAntR indeed showed its potential for intended deployments.

### 4.1 Resulting Design

Resulting robot, as shown in Figure 10, weights 2.2 kg when mounted with all legs, cabling and the Batterypack. In this setup, it is able to walk with at least additional mass of 1 kg, which is more than enough for intended onboard equipment. The overall cost of HAntR is around \$1100, as shown in Table 5, with the most expensive part being the servomotors used. In comparison to other design variants, we consider this price low; a slightly better XH-430 servomotor are already much more expensive. We experienced no significant problems during the manufacturing process or experiments described later. All parts proved as sufficiently resilient, exhibiting neglectable elasticity that would spoil the rigidity of the construction. Chosen PLA material endured experimental deployment with no signs of wearing, although part *Trochanter Knob* has been grazed slightly. But this grazing was caused by initial mounting due to a hole in part *Coxa Bracket* being printed imperfectly. (This part had to be printed with overhang, and therefore the plastic tended to drop slightly during printing.) After fitting *Trochanter Knob* into *Coxa Bracket* with exerting a slight force, imperfections grazed off and left a few marks of this process. Also, HAntR can be folded to several compact poses allowing a researcher to pack several robots and bring them to perform a field experiment, as shown in Figure 11.

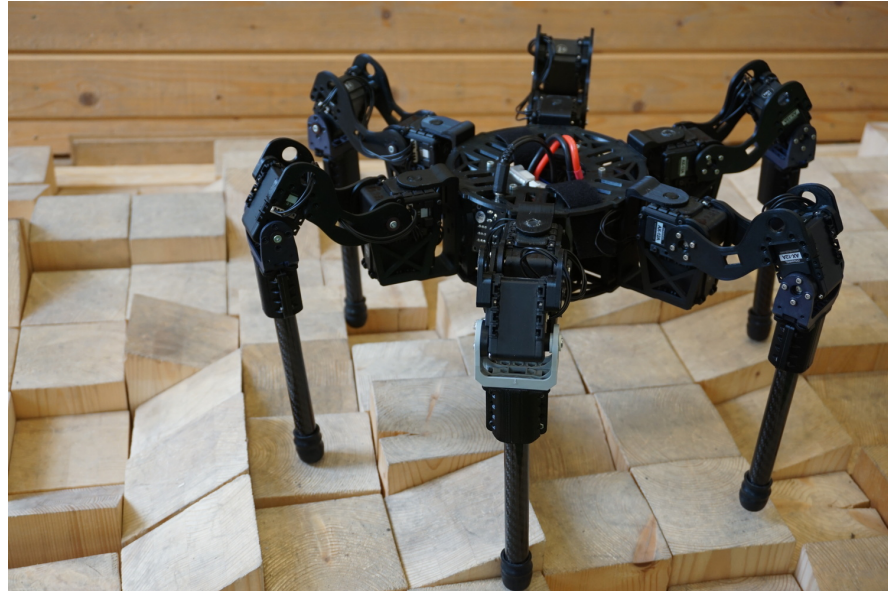


Figure 10: Photography of deployed HAntR.

Table 5: Building cost of HAntR.

Part	Quantity used	Unit cost [\$]	Total cost [\$]
AX-12A servomotor	24 pcs	37.4	897.6
PLA filament for 3D printing	~0.5 kg	18.0	9.0
Bioloid FP04-F2 bracket	6 pcs	0.6	3.8
Carbon tube	6 pcs	2.1	12.5
Rubber endings for <i>Foottip</i>	6 pcs	0.8	4.8
Basic circuitry for Daisy chain	1	-	20.0
Odroid-XU4	1	-	60.0
Li-Ion power cell	6	13.6	81.6
Total <sup>†</sup>			1132.0

<sup>†</sup> Approximately CZK 26000,-

#### 4.1 Known Mechanical Issues



Figure 11: Possible compact folding of legs.



Figure 12: IKT-proving experiment.

During months of HAntR’s being, it experienced several incidents like colliding its legs together due to erroneous code, tumbling from sloped terrain or hitting the ground with its feet too harshly because of a detuned positional threshold. Such mishaps performed on PhantomX often resulted to snapping some mechanical part or breaking servomotor gearbox due to torque too high. We may say, that so far neither any mechanical part nor any servomotor employed has been broken despite sometimes even tormenting conditions to which HAntR was subjected.

**Known Mechanical Issues** We have identified one significant systematic problem in our design. The cable leading between Coxa and Trochanter servomotors is endangered because servomotor AX-12A does not provide a way to lead it tightly along the axis of joint rotation. Instead, we had to take a long way around through an opening in *Servo Facing* and in a gap between *Servo Facing* and *Coxa Bracket*. This gap then imposed danger of cutting the cable. What is worse, when such an incident happens, repair takes about 20 min, because it involves dismounting and disassembling entire Trochanter with 24 screws. Movement of Coxa joint has to be further limited to angles between  $\pm 90^\circ$  to keep the cable perfectly safe. On the other hand, no other wiring issues have been observed as the wiring has been specifically designed such that there is only one more cable crossing some joint, moreover in this case imposing no danger.

We were not able to cut carbon tube precisely; lengths of individual Tibias altered by c.a. 2 mm, which resulted in imprecise IKT and DKT solutions because of both task solutions supposed ideal lengths of Tibias. Hence, the Denavit-Hartenberg parameters in Table 3 have to be calibrated. Our design also allows variable length of Tibia links by inserting Tibia Tube to Tibia Mount in different depths. Thus, such calibration can be performed in the future.

We know of PLA material property of softening with c.a.  $60^\circ\text{C}$ . Because of that, HAntR cannot be employed in warm conditions. We verified this property with an early version of part *Body Plate* of same black colour as of HAntR, which we used as a window lug in our laboratory. This part suffered from direct sunlight during the span of three months, which caused it to become so soft that we were able to bend it (not break it!) with bare hands. Therefore outdoor deployment of HAntR should be limited to at least shaded spaces, where no strong sunlight is present. Even though we think that HAntR, as is now, could be deployed in dirty or dusty environments, because of its passive long Tibias, which could protect the vulnerable torso from debris; this implies the potential of deployment.

As for free movements caused by too big gaps between adjacent mechanical parts, we consider such in our design as immeasurable by common tools ( $< 1^\circ$  per joint) and therefore neglectable. Above those small free movements were those induced by AX-12A imperfections most significant. Finally, 3 mm thick *Body Plate* bend approximately 1.5 mm under the pressure of studs holding it together, but luckily, it does not influence its function in any way.

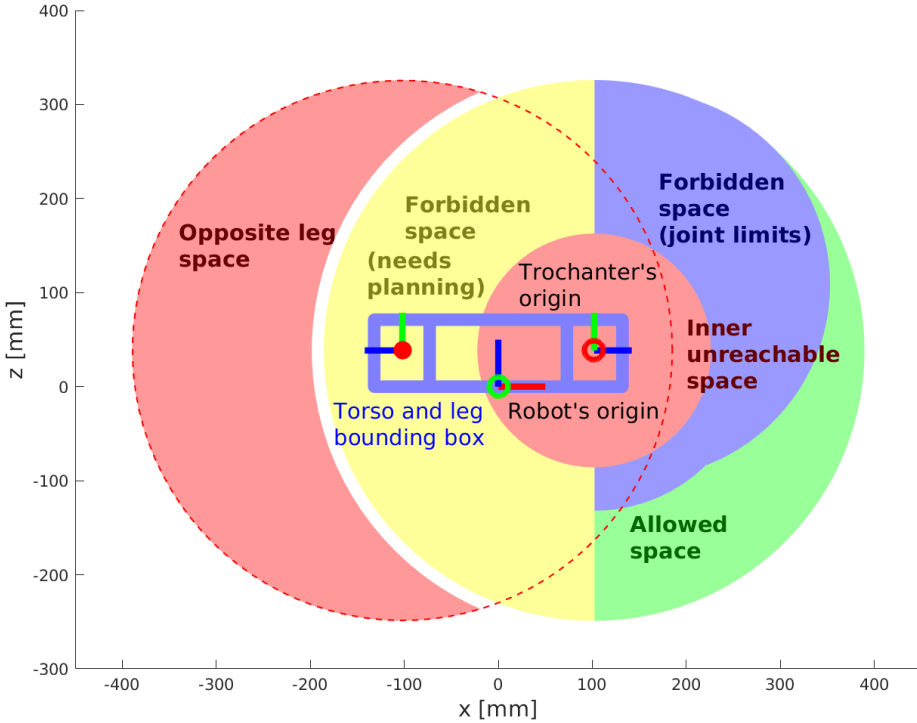


Figure 13: Visualisation of HAntR leg 0 operating space section in  $\mathcal{R}_0$   $xz$ -plane.

### 4.1.1 Verification of Kinematics

We proved qualitative correctness of IKT solver proposed in Section 3.2.2 by comparing results calculated and visualised in Matlab script with the real robot during this experiment. We chose one of the legs and moved others aside to make more space. We let HAntR sit still on supporting object, and we let its leg move to given points, as illustrated in Figure 12. Then we check whether foottip is in the vicinity of respective mark drawn on paper at a specific position using caliper and ruler. Current foottip can be approximated as a half-sphere with  $\sim 20$  mm diameter. Therefore measuring would be difficult because we had no precise reference point marked. Also, we knew about imperfections caused by manufacturing, and thus, exact measurements made no sense. Resulting differences from ordered positions never exceeded 20 mm, with joint coordinates resulting in the proposed single-out-of-four solution. Therefore, we may conclude that both IKT and DKT work correctly and may be utilised in following experiments. Moreover, we verified that the computation itself is fast as it is being executed under a millisecond thanks to the Eigen library.

Also, rather due to a need for demonstration of HAntR, we created a program which moves leg 0 along the outer frontier of its operating space. Because of discontinuity in joint space as described in 3.2.2 and lack of ingenious planning algorithm, we restrict our experiment only to  $z$ -positive side of  $J_2$   $xy$ -plane. From already observed simulations in Matlab, we see that the operating space forms approximately a convex spheroid reduced by smaller inner spheroid as illustrated in Figure 13. We prepared an interpolator for smooth leg movement.

The trajectory-generating procedure has the following parameters:  $z \in \mathbb{R}$  is the  $z$ -coordinate of plane w.r.t.  $\mathcal{R}_0$  in which foottip shall move.  $t \in \mathbb{R}$  is the time during which the trajectory shall be executed.  $t_p \in \mathbb{R}$  is the time between two consecutive interpolation events.  $o \in \{-1, 1\}$  is the direction of the interpolated trajectory. The number of interpolation steps is  $n = \frac{t}{t_p}$ .

## 4.2 Foot Strike Detection Using Positional Feedback Only



Figure 14: Photography of fixed-threshold derivation setup.

We define a pivot point  $P = [105, 0, z]$  which is a conveniently-chosen point for this experiment and a number of current interpolation step  $i \in \{0, 1, 2, s, n\}$ . From this point, we shall generate half-lines  $l$  from  $P$  in angles  $\alpha = o\frac{\pi}{2} - oi\frac{\pi}{n}$ . Those half-lines can be parameterised by  $u \in \mathbb{R}^+$  as

$$\forall X \in l : X = P + u[\cos \alpha, -\sin \alpha, 0]. \quad (20)$$

For each  $i$ , we set  $u_{start} = 100\,000$  mm which, is obviously an unsolvable position. Then we keep reducing  $u$  by step  $s = 30$  mm until we find a solvable case. When we find it, we return to last unsolvable  $u$  and reduce step  $s = s0.5$ . We repeat that until  $s$  becomes small enough, in our case  $s_{min} = 0.1$  mm. If  $u$  becomes negative, we may declare corresponding  $\alpha$  as totally unsolvable. This procedure finds the outer frontier of operational space with arbitrary resolution. By alternating signedness of  $s$  and starting point  $u_{start}$  we can get a generator for inner frontier.

## ■ 4.2 Foot Strike Detection Using Positional Feedback Only

To allow HAntR to perform walking and also according to thesis assignment, we were supposed to prove that the new robot can perform adaptive walking solely on information about the positional error on each joint. This problem represents a minimalist proprioceptive approach of foot strike detection, which was researched and proved on PhantomX robot [16, 46]. Foot strike detection is vital during movement in harsh terrain since it can reduce material stress significantly, prevent the robot from turning over or lessen vibrations induced by walking and hence stabilising cameras on robot torso, which is in its own right crucial for tasks relying on computer vision; without the adaptivity, robot would have to perform a fixed gait, which does not compensate for terrain irregularities. It relies on utilised Servomotor characteristics based mainly on low-level Positional controller. It means that after each new servomotor setpoint there is a regulating error  $\epsilon$  which is being eliminated by increased servomotor torque  $p\epsilon$ ,  $p$  being the regulating parameter; therefore, most of the time it operates with a nonzero error.

A controller relies on reading real joint coordinates immediately after writing them down. If the fast-enough response is achieved, we can get regulating error before it gets (at least partially) eliminated by servo-controller. We try to evaluate this regulating error with knowledge, that when

Table 6: Derived regulating error thresholds for adaptive gait.

Desired speed of foottip [m s <sup>-1</sup> ]	0.1	0.3	0.5	0.8
Proposed threshold [ticks]	10	25	35	60

foottip collides with the ground, resulting reactive force induces torques in each joint according to manipulator geometric Jacobian and hence increasing regulating error above some persistent level. We can say those leg collisions tended to create detectable features in regulating error signal; the features are however coupled with dynamics among all joint links. The signal feature detecting process can then be attended in several complexity-levels.

The easiest way is to set a fixed threshold for average regulating error on the entire leg and rely upon the error not exceeding the threshold during motion. This method needs finding such threshold which will not cause the leg to stop in midair (when the threshold is too low and triggers even during persistent regulating error) or to let robot to lift itself, when no leg collision is detected due to threshold too high. It was shown, that this method works acceptably on PhantomX robot.

Another method utilises a dynamic model of the leg to simulate how regulating error should look like in several next steps; according to that, a variable threshold is being set during runtime. If current manipulator Jacobian is utilised, we can get information about the direction of the reactive force and therefore sense collisions not only with the ground but with anything else. We chose the first mentioned method, since examining and deriving the dynamic model of the new robot is laborious, and due to limited available time, we were unable to squeeze another portion of work into this thesis.

We utilised the controller proposed in section 3.2.3. According to our previous observations, we set Femur joints to be read in the first place. That is because Femur joints carry most of the information about foot strike. (Force caused by colliding with flat ground gets distributed mostly on Femur servomotor which induces here biggest regulating error.) It was shown, that the controller frequency of 50 Hz is enough to control the robot.

### 4.2.1 Error Threshold Estimation

We tried to guess a fixed threshold by first commanding the robot to stay still with only a single leg swinging down in various angles ( $0^\circ, 45^\circ, -45^\circ$ ) and trajectories (straight down, sloped down and up). We gathered the data and plotted them in Figure 15 in several Cartesian foottip speeds. Resulting thresholds were estimated therefrom as shown in Table 6; the thresholds later proved as applicable for the task of in-place treading used in Section 4.3.1. An interesting fact can be noted: Previous PhantomX consistently experienced overshoots when a leg motion started [46]. However HAntR positional error signal seems not to have them, presumably due to lighter Tibia and related enhanced dynamics. the lowered gain then makes the dynamic system more stable. This fact may prove handy in the future, because it might be possible to compute an adaptive threshold not according to full leg dynamic model, but instead according to current geometric Jacobian.

### 4.2.2 Deployment in Locomotion Gait

Finally, we propose a seamless tripod gait with simple stride geometry, which tries to utilise as much of each leg operational space as possible. First, we determine which triplet of legs will be in support (phase S) according to Table 7. After capturing their position, we try to translate current supporting polygon as far against the required direction of travel as possible. We assume that robot will not

#### 4.2 Deployment in Locomotion Gait

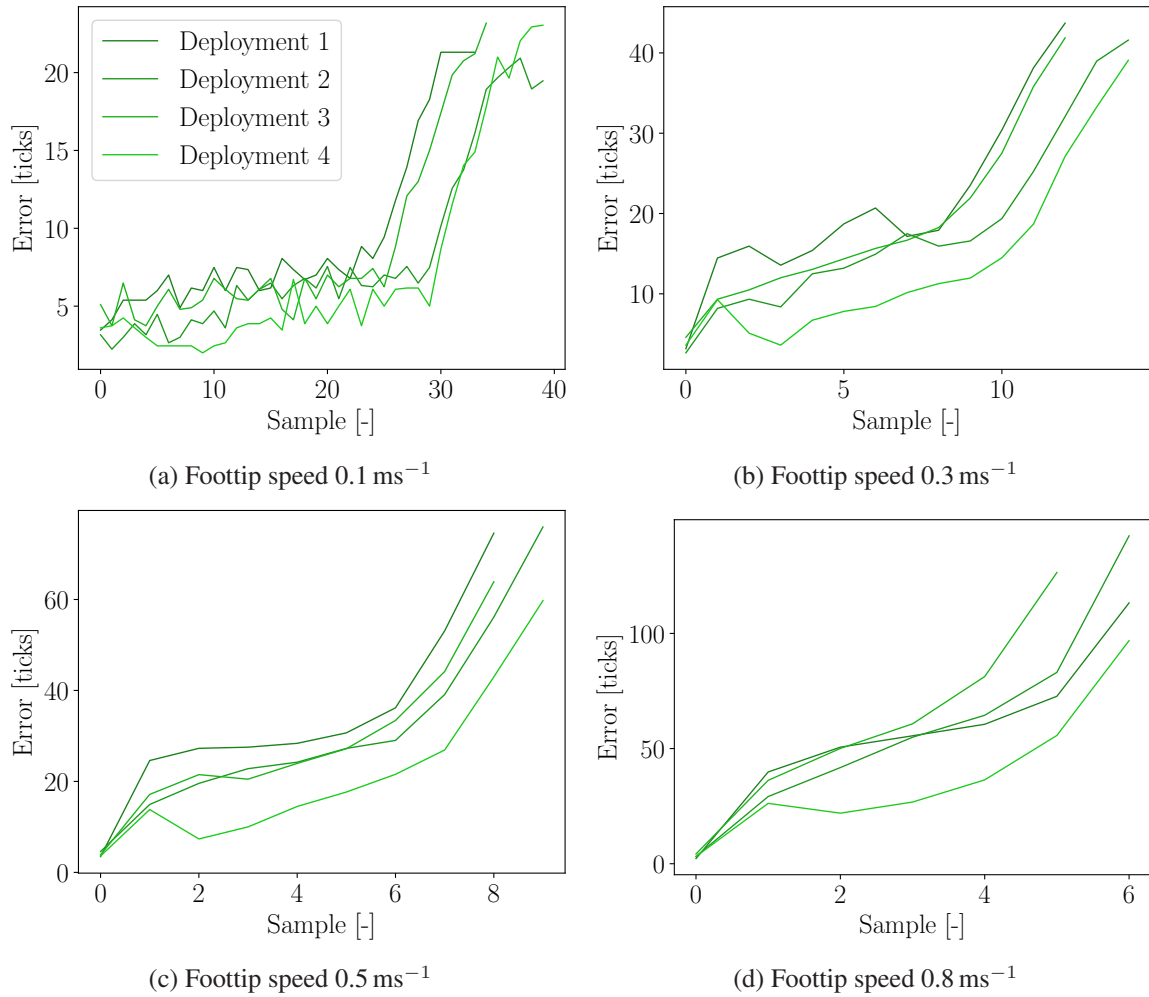


Figure 15: Regulating errors during static threshold derivation. The leg was forced to hit the floor in various orientations.

Table 7: Seamless tripod gait diagram.

Leg ID	Time						
	Stride 1			Stride 2			
0	S	S	S	A	B	C	
1	A	B	C	S	S	S	
2	S	S	S	A	B	C	
3	A	B	C	S	S	S	
4	S	S	S	A	B	C	
5	A	B	C	S	S	S	

walk in very harsh terrain and therefore neglecting yaw and roll rotations by assigning fixed resulting foottip height will prove good enough. (Since this experiment is focused on footstrike detection proof-of-concept, inaccuracies during support phase resulting in small slips do not matter.)

For the other three legs, we try to generate swing trajectory as three discrete segments. First, leg shall rise along a line directly up (phase A), then move along the direction of travel (phase B) and finally descend somewhat under the desired plane of supporting polygon to allow for collisions with delved footholds (phase C). In phase C, we employ the foot-strike detection method presented. During this phase, we also make the leg move against the direction of travel to get smoother contact with the ground. Immediately after we detect leg collision, we fix current position to former supporting legs and move that leg together with them until stride finishes. Support and swing legs then interchange and the next stride starts.

HAntR performed walk on a smooth surface with adaptive gait enabled and disabled. We measured HAntR torso height using a visual marker Apriltag attached to it. We presumed that adaptive gait enabled will lower variance in torso height.

Because HAntR experienced dynamic effects during the proposed gait, the proposed static threshold was not always helpful. Experiments strongly depended on the initial pose. From seven adaptive and six non-adaptive performed walks, we chose a particular case, when adaptive walk halved robot height variance as seen in Figure 16. We conclude that adaptive locomotion is possible, but especially during this faster type of gait needs some dynamic method of threshold computation.

## 4.3 Obtained Properties

With both the IKT and walking solved and proved, we have been able to finally verify even some runtime properties of HAntR. Following three experimental setups depict that our proposed robot introduces a major enhancement when compared to PhantomX robot and even when compared to other robots as already stated in Table 1.

### 4.3.1 Endurance and Temperature Test

We designed an experiment designed to show how long HAntR will be able to operate. The robot has been equipped with embedded computer Odroid-XU4 computing unit and fully charged 11.1 V Li-Poly battery with capacity of only 2600 mAh; in three executed experiments, HAntR lasted performing treading in place with simple footstrike detection for 61 min, 53 min and again 61 min. The second

#### 4.3 Endurance and Temperature Test

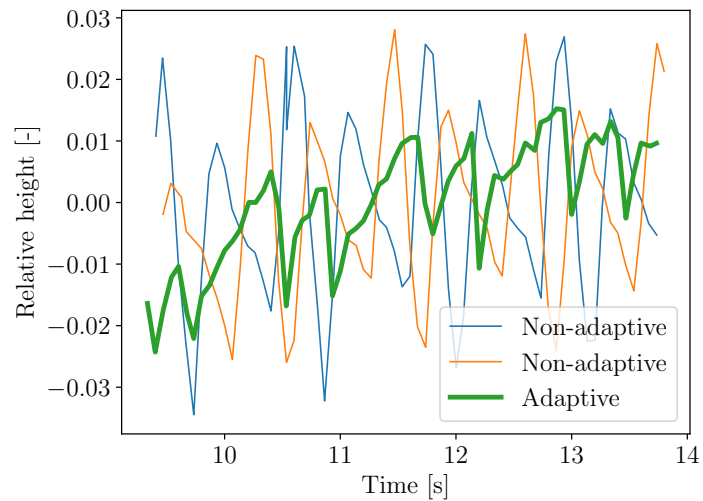


Figure 16: Graph of HAntR torso height during adaptive and non-adaptive walk.



Figure 17: Photography of HAntR performing treading in place.

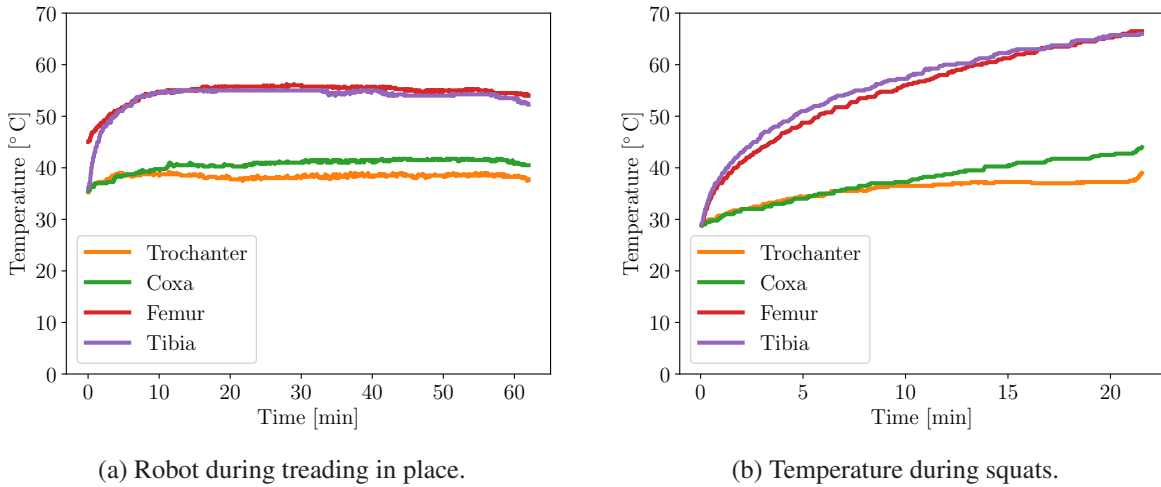


Figure 18: Temperature evolution in individual joints during endurance experiment in accumulated average values from all respective groups of servomotors reported.

run did not last as long, because we probably used a battery with its capacity already diminished. The treading had adaptive footstrike algorithm enabled and was designed to resemble a walk at a steady pace with foottips moving at a speed of  $0.15 \text{ m s}^{-1}$ . During the last run, before which the servomotors were left unloaded for 10 min to fan out, we also logged evolution of mean temperature in the servomotors; the temperature being directly relied to the servomotor torques, we wanted to see whether HAntR would be overloaded with operations or not. Figure 18a shows the evolution of the mean temperature of individual servomotor groups. We see that the temperature settles down; the steady temperature for Femur servomotor was c.a.  $55.4^\circ \text{ C}$  and for Tibia  $54.3^\circ \text{ C}$ . When compared to PhantomX [46], where a similar gait with a fixed threshold was deployed, we see that the temperatures are also similar. (C.a.  $55^\circ \text{ C}$  Femur and c.a.  $51^\circ \text{ C}$  Tibia.)

We also tried to emulate walking in a very rough environment. HAntR performed deep squats (body travelled 150 mm vertically with a velocity of  $0.15 \text{ m s}^{-1}$ ). During this experiment, a limiting factor was overheating of the servomotors; thus we conducted the experiment with off-board computation and off-board power supply. HAntR endured 22 min of continuous motion before some servomotors stalled because of overheat. The evolution of mean temperature of individual servomotors is depicted in Figure 18b. When compared to PhantomX, our robot can last for a longer period of time; PhantomX being loaded suffers from overheating in five minutes of walk.

### 4.3.2 Maximum Speed Test

We launched the robot five times with fixed seamless tripod gait and tried the maxim speed to obtain an idea about possibilities of HAntR. Using Apriltag system present we reconstructed robot's path, computed velocity, and filtered the results with 20-sample moving average. It was shown to us, that HAntR can walk as fast as  $0.424 (\pm 0.041) \text{ m s}^{-1}$ .

### 4.3.3 Variable-Steep Slope Adaption Test

This exercise is designed to show how the additional degree of freedom per leg helps HAntR with maintaining stability when standing on a sloped surface. Any rigid body is stable when its centre of mass projection in the direction of the gravitational vector to the gravity-perpendicular plane is inside its supporting polygon projection.

### 4.3 Variable-Steep Slope Adaption Test

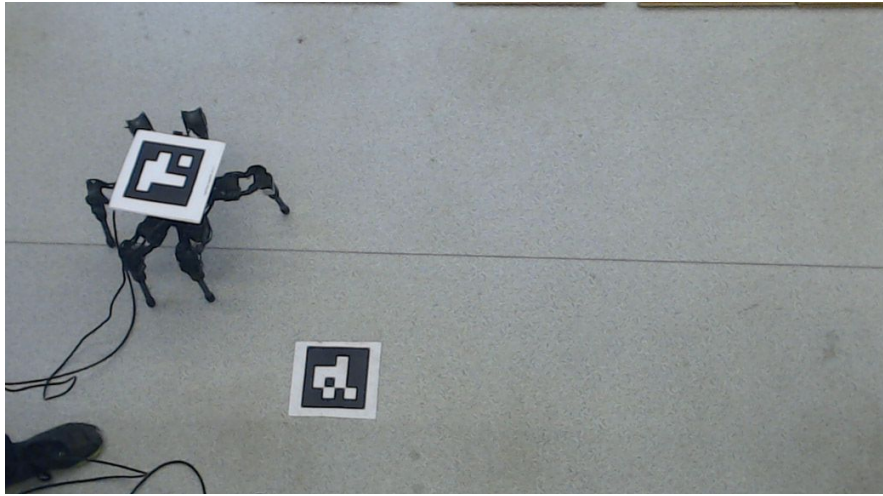


Figure 19: Image from a camera used for Apriltag localisation.

In this experiment, we compute supporting hexagon of circumscribed diameter  $r$  in a plane parallel to  $\mathcal{R}_0$   $xy$ -plane, offset along  $\mathcal{R}_0$   $z$ -axis by  $h$ ; this means that by changing supporting plane inclination, HAntR inclination will be changed accordingly. We move supporting plane in slow (quasistatic) motion. Therefore AX-12A servomotors are able to adapt position and orientation of HAntR with no significant dynamic effects involved. HAntR measures its orientation with an XSens MTi-30 AHRS unit capable of precise absolute (w.r.t. Earth gravity and magnetic field) yaw-pitch-roll orientation measurements. Resulting control loop computed new leg positions every 48 ms (20.8 Hz) which was in accordance with quasistatic motion. Apriltag system was also present. By computing difference of normal vectors of respective planes, we obtain real inclination of slope.

We conducted this experiment with  $r = 150$  mm,  $h = 150$  mm in two variants, at least five times each: The first variant had all joints enabled and was allowed to reach under the robot body to demonstrate full possibilities of the fourth joint. Whereas the second variant had fixed  $q_0 = 0$  (effectively reducing HAntR to 3 DoF kinematics) and limited leg operating space (forbidden reaching under torso) to emulate former PhantomX kinematics. We monitored both the angle in which HAntR began to fall over and joint regulating errors, which proportionally correspond to joint torque. Attention was paid for cables not to interfere with the results. We considered both the data and power cables to have neglectable impact on experiment, especially if held hanging loose.

Table 8: Maximum sustainable angles during slope balancing.

Experiment	Average angle [°]	Average Femur-Tibia error [ticks]
4 DoF	43.5	3.5
3 DoF	37.2	8.4

During running 4 DoF experiments, uneven lengths of Tibia Tube several times caused foottips to raise above supporting plane and thus data about positional errors became invalid. In the third run, we saw the experiment work properly. We present average captured position errors of Femur and Tibia during 4 DoF setup in Figure 20b compared against an illustrative example of 3 DoF setup in Figure 20a. Because the robot achieved inclination below  $45^\circ$ , these two servomotors carried most of the information because; the other two were mainly supported by passive reaction force. From the example it is clear, that fourth DoF helped HAntR with shifting its centre of mass and thus dividing

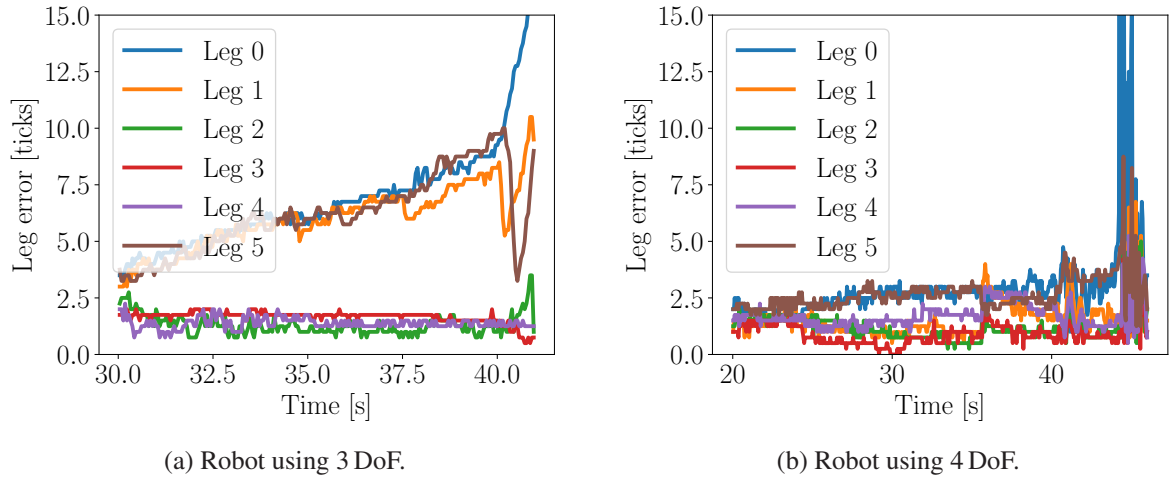


Figure 20: Comparison of average positional errors on Femur and Tibia servomotors for each leg during both types of experiments.

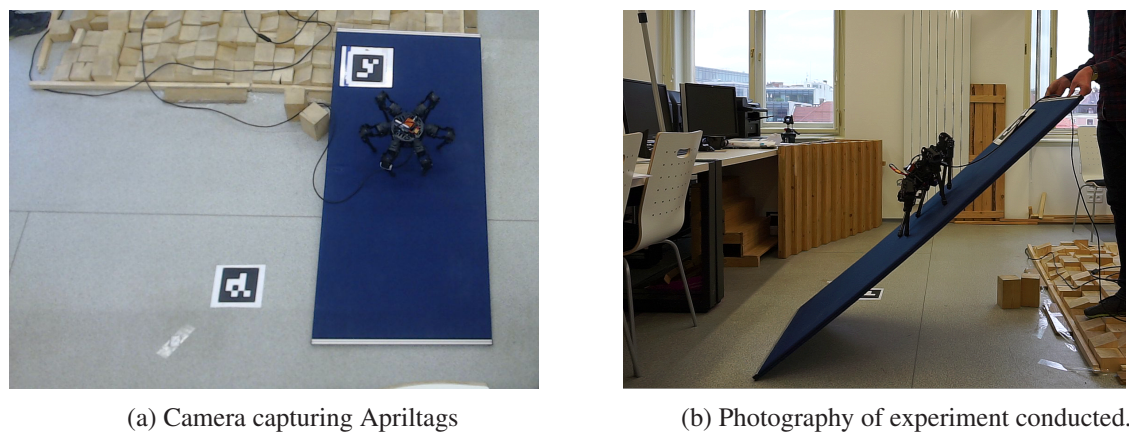


Figure 21: Photography of slope balancing experiment.

#### *4.3 Variable-Steep Slope Adaption Test*

overall stress onto all legs as opposed to 3 DoF, which reached its limit shortly and then more stress was distributed to lower legs. As to angles reached, 4 DoF emerged as a better sustainer by only  $5^\circ$  on average. However, all experiments terminated not by HAntR reaching unstable pose, but rather by exceeding static friction force and thus slipping down. Much better force distribution than caused slightly better result of 4<sup>th</sup> DoF.

We have presented results of our work in this Section. We provide a sample portions of code, most importantly the IKT and DKT implementation on the attached CD for the reader to be able to replicate the results. We have run the code under Unix/Linux Ubuntu 18.04 operating system and we advise the reader to do the same in order to achieve the same functionality. To compile the codes correctly obtaining executable binaries, both Bioloid controller library [57] and Eigen library [59] have to be present but are not provided with our code. HAntR has to be connected to the computer via a serial interface, in our case USB later converted to Dynamixel daisy chain signal. The code is able to lookup connected robot and possibly also Xsens sensor among `dev/ttyUSB0`–`dev/ttyUSB4` interfaces.

## Chapter 5

# Conclusion

We were able to design, construct and verify entirely new robot HAntR according to list of Specifications presented in Section 2. The individual specifications were fulfilled as follows.

Specification 1 was fulfilled by enhancing the leg with an additional joint, achieving a kinematic chain with 4 DoF. We changed the assigned yaw-roll-pitch-pitch configuration to roll-yaw-pitch-pitch; this change was mainly implied by several other requirements to robot design, such as Specification 4—a compact design. The resulting leg which by its very nature enables foreign bodies manipulations was also proven to help with sloped surface balancing in Section 4.3.3. This possibility of force-vectorisation is expected to enhance slope walking, obstacle negotiation or any-angle tactile sensing. Even though our current solution still has kinematic limitations as written in Section 3.2.2, the robot was able to perform adaptive walking. Moreover, measured maximum speed with no significant gait optimisations was as high as  $0.42 \text{ m s}^{-1}$ . As described in Section 3.1.1, the leg itself is detachable from the torso and can be replaced by a compatible leg.

Specification 2 was achieved by crafting Tibia from diameter 16 mm carbon fibre tube, as shown in Section 3.1.1. The tube, having an inner diameter of c.a. 15 mm, may support additional sensory and safe cable wiring. The *Foottip* made from rubber endings endured HAntR deployment so far with no signs of wearing. When compared to the former PhantomX robot, new foottip already endured longer. Since the foottip diameter is c.a. 20 mm, half the former design, it also achieves demand on small size.

Requirements of Specification 3 were solved simply by designing such a torso, that had made all the legs equivalent, as shown in Section 3.1.2. Such design resulted in the robot which, when not equipped with unidirectional sensory, was truly omnidirectional.

Specification 4 was achieved by a complete overhaul of former PhantomX leg and torso with carefully considered enhancement of mass distribution, as shown in Sections 3.1.1 and 3.1.2. By making Tibia longer than Femur, we also allowed HAntR to operate in a near-passive pose. When combined, resulting robot was able to operate for around an hour before it run out of energy, despite being equipped with an inferior battery with half the designed capacity. The design proved as feasible because the robot was able to operate without a danger of overheating; indeed in [27] it is stated, that naive approach of the fourth DoF as shown in Figure 5b results in torques too high for AX-12A servomotors. Lowered joint torques also resulted in fewer servomotor causalities. Finally, HAntR also offers a possibility to fold itself in a compact pose allowing easy transportation.

In the thesis, solutions of both inverse and direct kinematic tasks required by Specification 5 were solved in Section 3.2. Proposed DKT formulation allows computation of any leg link position, which could be later utilised in various problems, such as enhanced collision-avoidance or dynamic simulation. IKT then yields valid solutions, as shown in Section 4.1.1. The solution is aware of singularities and numerical pitfalls; the singularities are forbidden to happen at all, spots of possible numerical inaccuracies are either named or forbidden and may be further negotiated.

The electronic design required in Specification 6 was also achieved. Odroid-XU4 with Li-Poly battery can be currently attached with Velcro straps. Current design offers the possibility to create a scaffolding for other electronics by slightly redesigning *Body Plate* in the future. The presented design also provides a way of safe cable wiring except for the path between Coxa and Trochanter servomotor. This part is a major threat to our robot because the cable may be torn by improper actuation. Coxa movement has to be limited by values in Table 4 to prevent tedious surgery.

## 5.1 Future Work

It is possible to fit at least six Li-Ion cells with a total capacity of at least 66.6 Wh, as shown in Section 3.1.2. The primary six-tuple of cells is designed to fit in a Batterypack which in turn fits inside the robot and can be simply replaced. Other triplets can be added with up to 12 cells; 18 cells could be also present, but with the need for nontrivial torso modification.

We developed a software implementing both IKT and DKT as required in Specification 8; it also enables direct servo commanding and utilities like raw read and write operations or joint-space and temperature logger. Collision detector respecting limitations in Table 4 was also successfully employed.

Specification 9 required better material and design process. Fusion360 proved as a good design tool despite some drawbacks, e.g., that the most important files of the design were not under our control; but after all, designing the robot was swift and intuitive once we got acquainted with offered design tools. Besides, Fusion360 provided us with fancy rendering utility which we used to make the renderings in this thesis. Regarding the material choice, PLA plastic was sufficient to the degree of indoor experimental deployment; it sustained even quite harsh conditions when the robot fell from a heightened surface during slope-balancing or when it clashed its legs together. Moreover, if any printed part ever came to harm, we can replace it by another one which could be reprinted in terms of a few hours at most. Carbon fibre tube also resisted all the impacts and we may conclude that it may be further used in possible other versions of robots.

Finally, in Section 4 and following Specification 10, we showed that fourth degree of freedom, implemented in the proposed design, indeed enhanced the motion capabilities of the robot. Although having weight increased by c.a. 300 g, the robot was able to endure walking-like action longer than comparable hexapods, as shown in Table 1. The only two robots better than HAntR were RHex and Hexie; but both of them sacrificed either its terrain traversability or payload weight, whereas HAntR kept and even enhanced both of it. We also shown that adaptive walking algorithm is possible with HAntR. Summed together, we believe that the assignment of the thesis was successfully fulfilled.

## 5.1 Future Work

The most important task after finishing this thesis is extending the current controller so it can locomote HAntR according to given arbitrary velocity command. The controller should be later enhanced in a way that utilises full potential of 4 DoF kinematics; one of the most significant upgrades is enabling lateral leg lift, which allows for rougher terrain navigation. After achieving this, HAntR should be able to participate in DARPA Subterranean challenge [60].

Enhanced leg-leg and leg-body collision detector allowing leg movements even in adjacent leg operating space will be needed; a low-resolution polyhedron model could be employed. Then various other methods of gait-performing can be implemented, e.g., explicit motion planning [61]; such an approach can further be extended to optimal locomotion planning. The controller could also be formulated as a hybrid dynamic system with several plug-in controllers and modules determining footstrikes, slips, collisions, or failures.

We should perform torque analysis experiment [26] on HAntR, and compare rigorous results with other robots. Also, we would like to create a demonstrator of its manipulative capabilities.

We need to derive the geometric Jacobian which will enable static force-control in leg foottips and probably even provide an adaptive threshold for position-feedback only locomotion. Afterwards, whole dynamic model should be derived; this would allow for energy-optimal motion planning, robust control, better velocity command response and more.

We intend to negotiate the problem of Trochanter-Coxa cable path in a future robot utilising Dynamixel X-Series servomotors, which is also made of more durable material. This robot shall also have debris-proof torso made of better material making it suitable to dusty, wet or warm environment. Mechanical design and manufacturing will be done according to professional standards and thus imperfections observed with HAntR shall not be present.

As to HAntR itself, we plan to create several other exemplars for ComRob ongoing research. Also, we might develop a branch version utilising only 3 DoF both for comparison and robust deployment. All of these robots could benefit from FPGA-based communications accelerator [43]. A fact, that all of the parts are replaceable inspires consequent design ideas: A compliant Femur link, possibly with optimised length could be tried. An idea of passive Tarsus joint, which could enhance adhesion as well as enable another approach of tactile sensing also emerged. On top of *Body Plate*, we may fit a rotating turret, which could carry an RGBD camera; this could at least partially compensate vibrations induced by robot gait and also return omnidirectionality lost with an unidirectional camera. A camera with a “fish-eye” lens could be mounted either on top of the robot or the bottom, effectively achieving 360° field of view and possibly offering visual odometry in the latter case. An integrated, possibly wireless, charging system should enable long-term or multi-robot deployments.

We would also like to dive into other robotic topics: Furnishing a robot with optical markers attached to each joint or link could enable a gesture-based communication or precise localisation. Short range selective communication via infrared transceivers, a set of cameras, together covering full robot radius, or various other electronics can be placed between legs. (See Figure 7, yellow cylinders.) Haptic exploration could be used as a mean of navigation in a very rough environment with degraded sensing where standard optic or radio methods fail.

## References

- [1] K. Čapek. *R.U.R.: Rossumovi univerzální roboti*. Aventinum, 1920.
- [2] B. Siciliano, L. Sciavicco, L. Villani, and G. Oriolo. *Robotics: Modelling, Planning and Control*. Advanced Textbooks in Control and Signal Processing. Springer London, 2009.
- [3] R. Welch, D. Limonadi, and R. Manning. Systems engineering the Curiosity Rover: A retrospective. In *8th International Conference on System of Systems Engineering*, pages 70–75, 2013.
- [4] T. McGeer. Passive walking with knees. In *IEEE International Conference on Robotics and Automation (ICRA)*, volume 3, pages 1640–1645, 1990.
- [5] J. Liu, M. Tan, and X. Zhao. Legged robots — an overview. *Transactions of the Institute of Measurement and Control*, 29(2):185–202, 2007.
- [6] H. Nozaki, Y. Kujirai, R. Niiyama, Y. Kawahara, T. Yonezawa, and J. Nakazawa. Continuous shape changing locomotion of 32-legged spherical robot. In *IEEE/RSJ International Conference on Intelligent Robots and Systems (IROS)*, pages 2721–2726, 2018.
- [7] C. Paul, J. W. Roberts, H. Lipson, and F. J. Valero Cuevas. Gait production in a tensegrity based robot. In *12th International Conference on Advanced Robotics*, pages 216–222, July 2005.
- [8] Lukáš Černý, Petr Čížek, and Jan Faigl. On evaluation of motion gaits energy efficiency with a hexapod crawling robot. In *Acta Polytechnica CTU Proceedings*, volume 6, pages 6–10, 2016.
- [9] M. Rubenstein, C. Ahler, N. Hoff, A. Cabrera, and R. Nagpal. Kilobot: A low cost robot with scalable operations designed for collective behaviors. *Robotics and Autonomous Systems*, 62(7):966–975, 2014.
- [10] S. Kornienko, O. Kornienko, A. Nagarathinam, and P. Levi. From real robot swarm to evolutionary multi-robot organism. In *IEEE Congress on Evolutionary Computation*, pages 1483–1490, 2007.
- [11] S. Huh, U. Lee, H. Shim, J. Park, and J. Noh. Development of an unmanned coal mining robot and a tele-operation system. In *11th International Conference on Control, Automation and Systems*, pages 31–35, 2011.
- [12] M. Hutter, C. Gehring, A. Lauber, F. Gunther, C. D. Bellicoso, V. Tsounis, P. Fankhauser, R. Diethelm, S. Bachmann, M. Bloesch, H. Kolenbach, M. Bjelonic, L. Isler, and K. Meyer. Anymal — toward legged robots for harsh environments. *Advanced Robotics*, 31(17):918–931, 2017.
- [13] G. Bledt, M. J. Powell, B. Katz, J. Di Carlo, P. M. Wensing, and S. Kim. Mit cheetah 3: Design and control of a robust, dynamic quadruped robot. In *IEEE/RSJ International Conference on Intelligent Robots and Systems (IROS)*, pages 2245–2252, 2018.
- [14] Collective of Authors. Anymal technology specification leaflet. URL: <https://www.anybotics.com/anymal-legged-robot/>. Cited on 2019-05-13.
- [15] M. W. Spong and M. Vidyasagar. *Robot dynamics and control*. Wiley, 2004.

- [16] J. Mrva and J. Faigl. Tactile sensing with servo drives feedback only for blind hexapod walking robot. In *10th International Workshop on Robot Motion and Control (RoMoCo)*, pages 240–245, 2015.
- [17] M. Bjelonic, N. Kottege, and P. Beckerle. Proprioceptive control of an over-actuated hexapod robot in unstructured terrain. In *IEEE/RSJ International Conference on Intelligent Robots and Systems (IROS)*, pages 2042–2049, 2016.
- [18] T. Buettner, A. Roennau, G. Heppner, and R. Dillmann. Design of an exchangeable, compact and modular bio-inspired leg for six-legged walking robots. In *Human-Centric Robotics*, pages 89–96, 2017.
- [19] Interbotics. PhantomX Mark II hexapod. URL: <https://www.trossenrobotics.com/phantomx-ax-hexapod.aspx>. Cited on 2019-05-01.
- [20] F. Tedeschi and G. Carbone. Design issues for hexapod walking robots. *Robotics*, 3(2):181–206, 2014.
- [21] K. Galloway, G. Clark Haynes, D. Ilhan, A. M. Johnson, R. Knopf, G. A. Lynch, B. N Plotnick, M. White, and D. Koditschek. X-RHex: A Highly Mobile Hexapedal Robot for Sensorimotor Tasks. *Technical Reports (ESE)*, 2010.
- [22] D. Belter and K. Walas. A compact walking robot–flexible research and development platform. In *Recent Advances in Automation, Robotics and Measuring Techniques*, pages 343–352. Springer, 2014.
- [23] M. Gorner, T. Wimbock, A. Baumann, M. Fuchs, T. Bahls, M. Grebenstein, C. Borst, J. Butterfass, and G. Hirzinger. The DLR-Crawler: A testbed for actively compliant hexapod walking based on the fingers of DLR-Hand II. In *IEEE/RSJ International Conference on Intelligent Robots and Systems (IROS)*, pages 1525–1531, 2008.
- [24] S. Kalouche, D. Rollinson, and H. Choset. Modularity for maximum mobility and manipulation: Control of a reconfigurable legged robot with series-elastic actuators. In *IEEE International Symposium on Safety, Security, and Rescue Robotics (SSRR)*, pages 1–8, 2015.
- [25] Collective of Authors. HEBI Robotics. URL: [http://docs.hebi.us/resources/kits/assyInstructions/A-2049-01\\_Data\\_Sheet.pdf](http://docs.hebi.us/resources/kits/assyInstructions/A-2049-01_Data_Sheet.pdf). Cited on 2019-05-01.
- [26] M. T. Nguyenová. High-fidelity modeling of hexapod walking robot locomotion. Bachelor’s thesis, Czech Technical University in Prague, Faculty of Electrical Engineering, 2019.
- [27] O. A Silva, P. Sigel, W. Eaton, C. Osorio, E. Valdivia, N. Frois, and F. Vera. CRABOT: A six-legged platform for environmental exploration and object manipulation. In *Proceedings of the 4th Congress on Robotics and Neuroscience*, pages 46–51, 2018.
- [28] A. Roennau, G. Heppner, M. Nowicki, and R. Dillmann. LAURON V: A versatile six-legged walking robot with advanced maneuverability. In *IEEE/ASME International Conference on Advanced Intelligent Mechatronics*, pages 82–87, 2014.
- [29] T. M. Roehr, F. Cordes, and F. Kirchner. Reconfigurable Integrated Multirobot Exploration System (RIMRES): Heterogeneous Modular Reconfigurable Robots for Space Exploration. *Journal of Field Robotics*, 31(1):3–34, 2014.

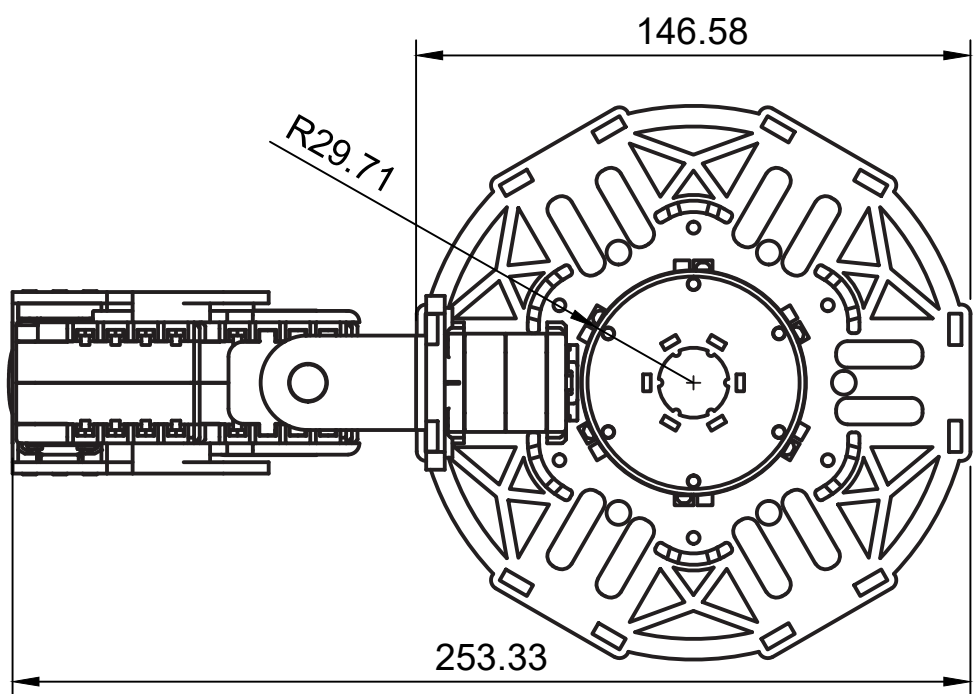
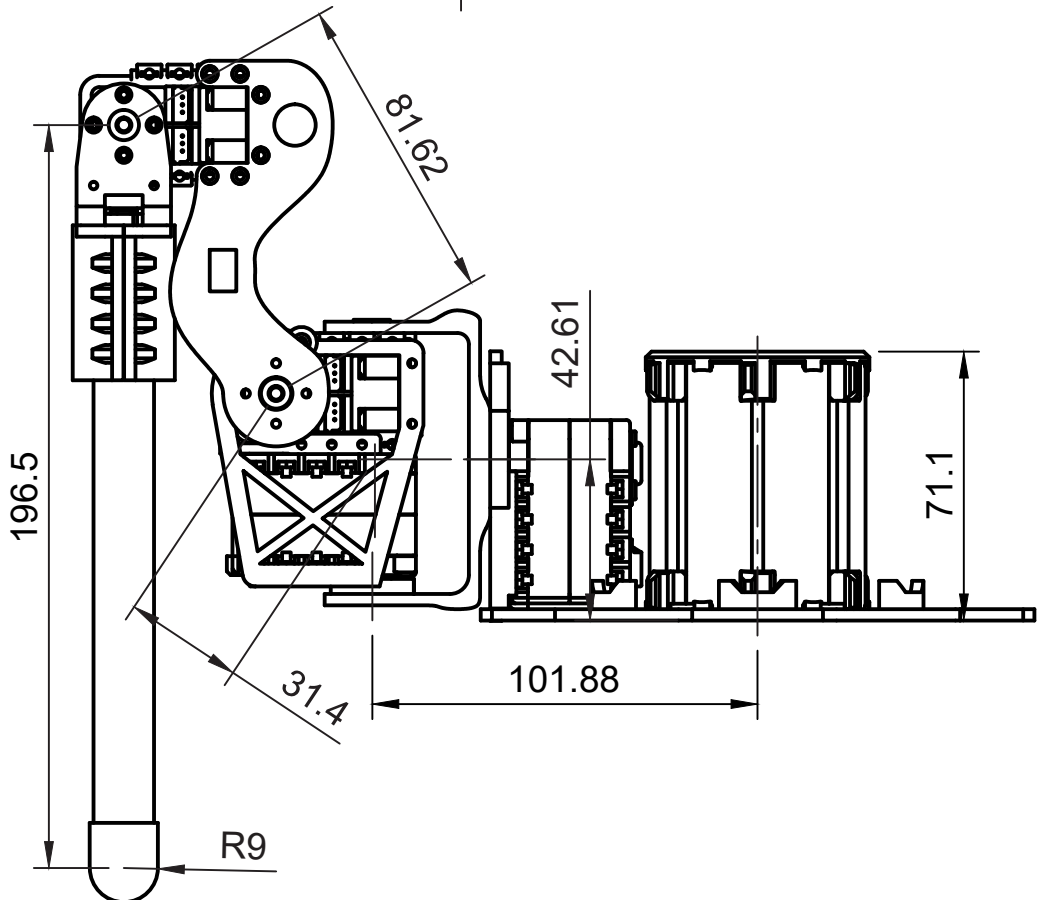
- [30] M. Bjelonic, N. Kottege, T. Homberger, P. Borges, P. Beckerle, and M. Chli. Weaver: Hexapod robot for autonomous navigation on unstructured terrain. *Journal of Field Robotics*, 35(7):1063–1079, 2018.
- [31] Vorpal Robotics LLC. Vorpal the Hexapod. URL: [http://vorpalrobotics.com/wiki/index.php/Vorpal\\_The\\_Hexapod](http://vorpalrobotics.com/wiki/index.php/Vorpal_The_Hexapod). Cited on 2019-05-14.
- [32] J. Dupeyroux, J. R. Serres, and S. Viollet. Antbot: A six-legged walking robot able to home like desert ants in outdoor environments. *Science Robotics*, 4(27), 2019.
- [33] Kåre Halvorsen. MorphHex Mark III. URL: <http://zentasrobots.com/robot-projects/morphhex-part-1/>. Cited on 2019-05-14.
- [34] G. Passault, Q. Rouxel, F. Petit, and O. Ly. Metabot: A low-cost legged robotics platform for education. In *International Conference on Autonomous Robot Systems and Competitions (ICARSC)*, pages 283–287, 2016.
- [35] ArcBotics. Hexy the Hexapod. URL: <http://arcbotics.com/products/hexy/>. Cited on 2019-05-14.
- [36] Collective of Authors. Hexa. URL: <https://www.vincross.com/hexa>. Cited on 2019-05-18.
- [37] J. Sun and J. Zhao. An adaptive walking robot with reconfigurable mechanisms using shape morphing joints. *IEEE Robotics and Automation Letters*, 4(2):724–731, 2019.
- [38] K. Walas. Foot design for a hexapod walking robot. *Pomiary, Automatyka, Robotyka*, 17(2):283–287, 2013.
- [39] P. Čížek, J. Kubík, and J. Faigl. Online foot-strike detection using inertial measurements for multi-legged walking robots. In *IEEE/RSJ International Conference on Intelligent Robots and Systems (IROS)*, pages 7622–7627, 2018.
- [40] K. Berns, S. Cordes, and W. Ilg. Adaptive, neural control architecture for the walking machine LAURON. In *IEEE/RSJ International Conference on Intelligent Robots and Systems (IROS)*, volume 2, pages 1172–1177, 1994.
- [41] S. Feng, E. Whitman, X. Xinjilefu, and C. G. Atkeson. Optimization based full body control for the atlas robot. In *IEEE-RAS International Conference on Humanoid Robots*, pages 120–127, 2014.
- [42] Collective of Authors. Dynamixel AX-12A servomotor electronic datasheet. URL: <http://emanual.robotis.com/docs/en/dxl/ax/ax-12a/>. Cited on 2019-05-01.
- [43] M. Tržil. FPGA-based control of multi-legged walking robot. Bachelor’s thesis, Czech Technical University in Prague, Faculty of Electrical Engineering, 2019.
- [44] Collective of Authors. Robot Cable-3P Set BCS-3P01. URL: <http://www.robotis.us/robot-cable-3p-set-bcs-3p01/>. Cited on 2019-05-16.
- [45] Technical Committee ISO/TC 1. ISO general purpose metric screw threads – Selected sizes for screws, bolts and nuts. Standard, International Organization for Standardization, 1998.
- [46] J. Faigl and P. Čížek. Adaptive locomotion control of hexapod walking robot for traversing rough terrains with position feedback only. *Robotics and Autonomous Systems*, 116:136–147, 2019.

- [47] Robotics and Autonomous Systems Group — CSIRO. Weaver: Hexapod robot with 5DoF limbs for navigating on unstructured terrain. URL: <https://research.csiro.au/robotics/weaver/>. Cited on 2019-05-16.
- [48] Image of Six-legged walking robot LAURON V from the FZI Research Center for Information Technology in Karlsruhe, Germany. URL: <https://en.wikipedia.org/wiki/LAURON>. Cited on 2019-05-16.
- [49] J. Collins, B. Cottier, and D. Howard. Comparing direct and indirect representations for environment-specific robot component design. *Clinical Orthopaedics and Related Research*, abs/1901.06775, 2019.
- [50] USB-IF. USB Implementers Forum Webpage. URL: <https://www.usb.org/>. Cited on 2019-05-18.
- [51] Collective of Authors. OpenSCAD. URL: <http://www.openscad.org/>. Cited on 2019-05-18.
- [52] Collective of Authors. GIT. URL: <https://git-scm.com/>. Cited on 2019-05-18.
- [53] The Apache Software Foundation. Subversion. URL: <https://subversion.apache.org/>. Cited on 2019-05-18.
- [54] Collective of Authors. Fusion360. URL: <https://www.autodesk.com/products/fusion-360/>. Cited on 2019-05-18.
- [55] J. Průša. Základy 3D tisku. URL: <https://www.prusa3d.cz/kniha-zaklady-3d-tisku-josefa-prusi/>. Cited on 2019-05-13.
- [56] Collective of authors. Ieee standard for floating-point arithmetic. *IEEE Std 754*, pages 1–70, 2008.
- [57] Vanadium Labs. Bioloid controller library repository. URL: <https://github.com/vanadiumlabs/arbotix/tree/master/libraries/Bioloid>. Cited on 2019-05-18.
- [58] E. Olson. Apriltag: A robust and flexible visual fiducial system. In *IEEE International Conference on Robotics and Automation (ICRA)*, pages 3400–3407, 2011.
- [59] Collective of Authors. Eigen library. URL: [http://eigen.tuxfamily.org/index.php?title=Main\\_Page](http://eigen.tuxfamily.org/index.php?title=Main_Page). Cited on 2019-05-19.
- [60] Defense Advanced Research Projects Agency. DARPA Subterranean Challenge Webpage. URL: <https://www.subtchallenge.com/>. Cited on 2019-05-18.
- [61] P. Čížek, D. Masri, and J. Faigl. Foothold placement planning with a hexapod crawling robot. In *IEEE/RSJ International Conference on Intelligent Robots and Systems (IROS)*, pages 4096–4101, 2017.

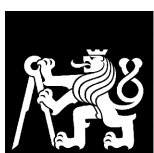
## **Appendix A**

# **Mechanical Design Blueprints**

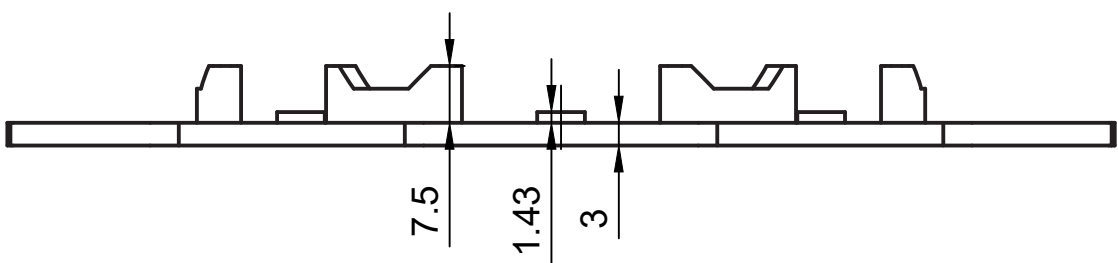
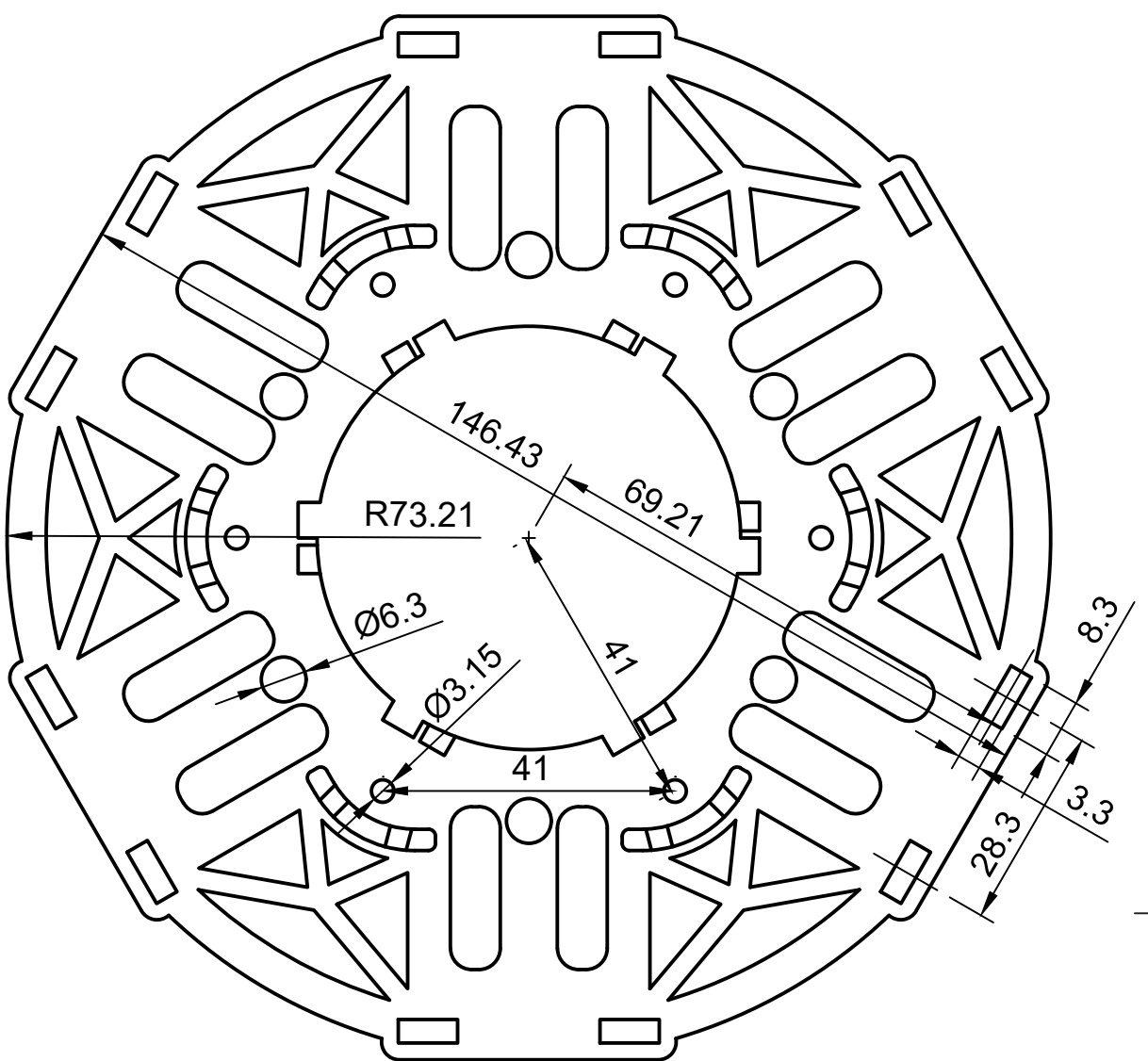
A technical documentation exported from Fusion360 CAD software in a defined scale can be found on the following pages. All considered mechanical parts with important dimensions are depicted. On Compact Disk attached to this thesis, the design is also available in STL file format.



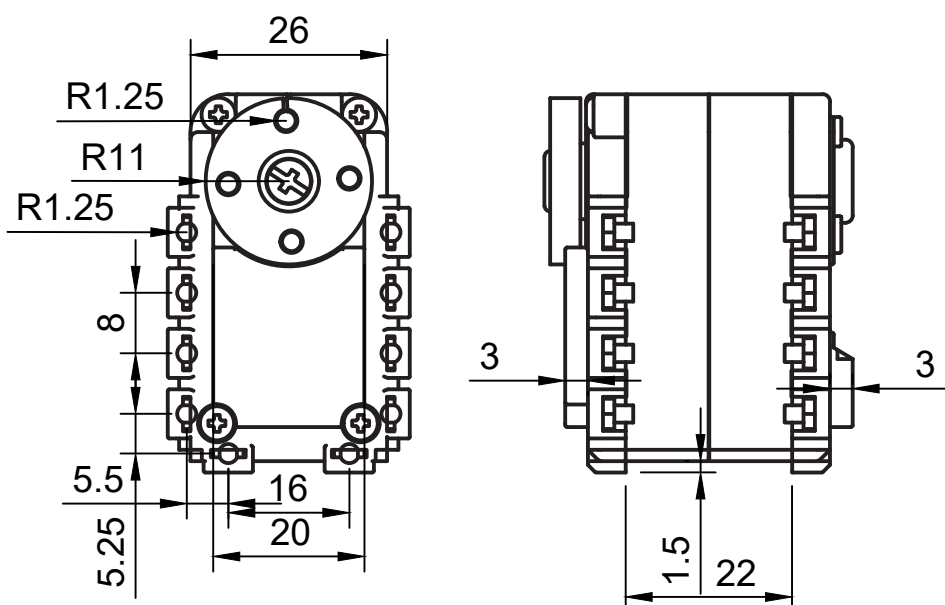
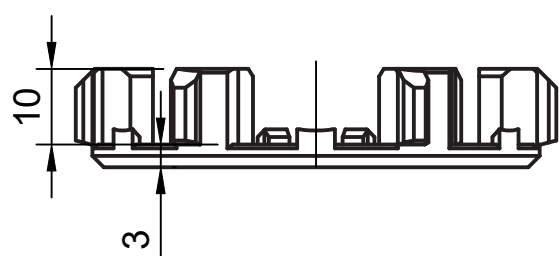
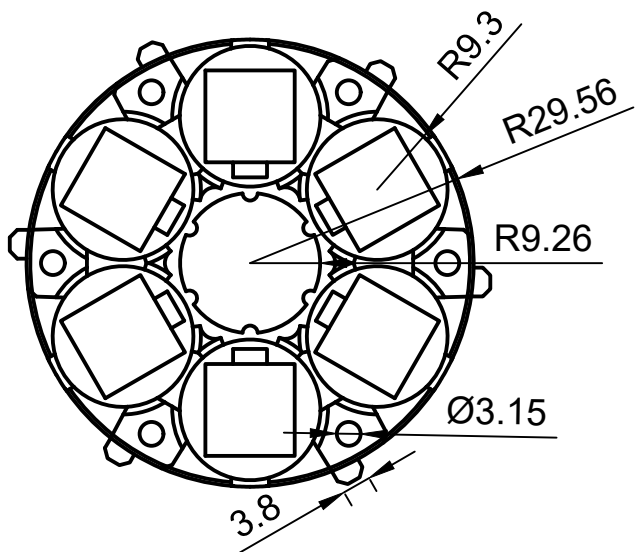
Dept. ComRob	Scale 1:2	Created by Martin Zoula, 10.5.2019	Approved by
		Document type Technical Documentation	Document status
		Title HAntR Hexapod Robot Mechanical Design Situation overview	DWG No.
		Rev. 1	Date of issue 24.5.2019
		Sheet 1/6	



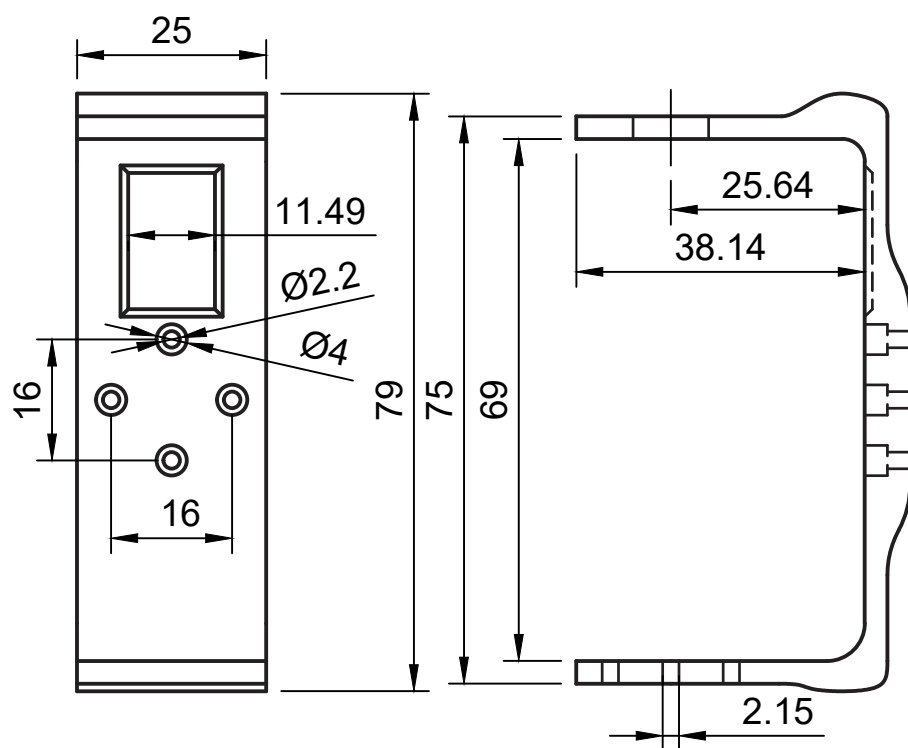
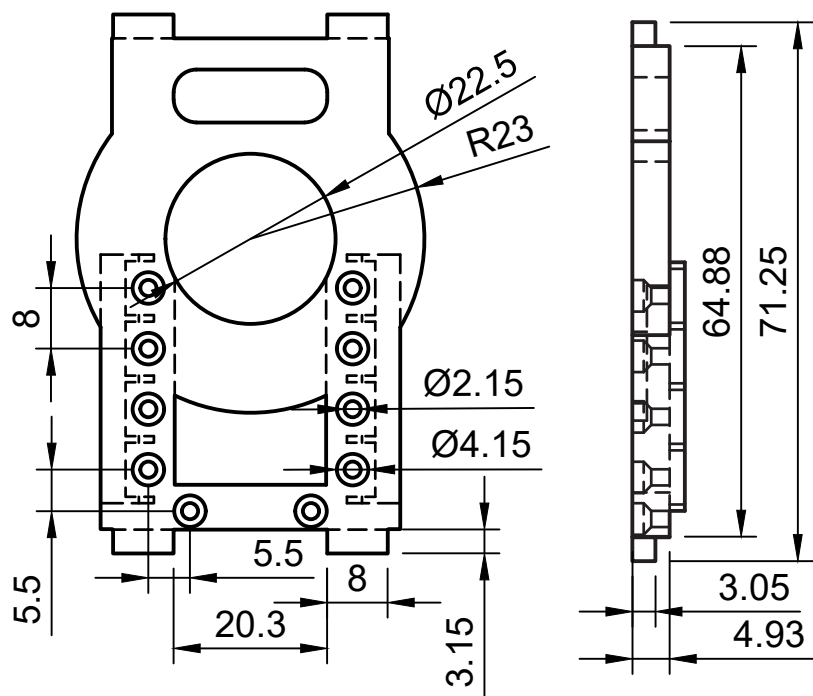
**FACULTY  
OF ELECTRICAL  
ENGINEERING  
CTU IN PRAGUE**



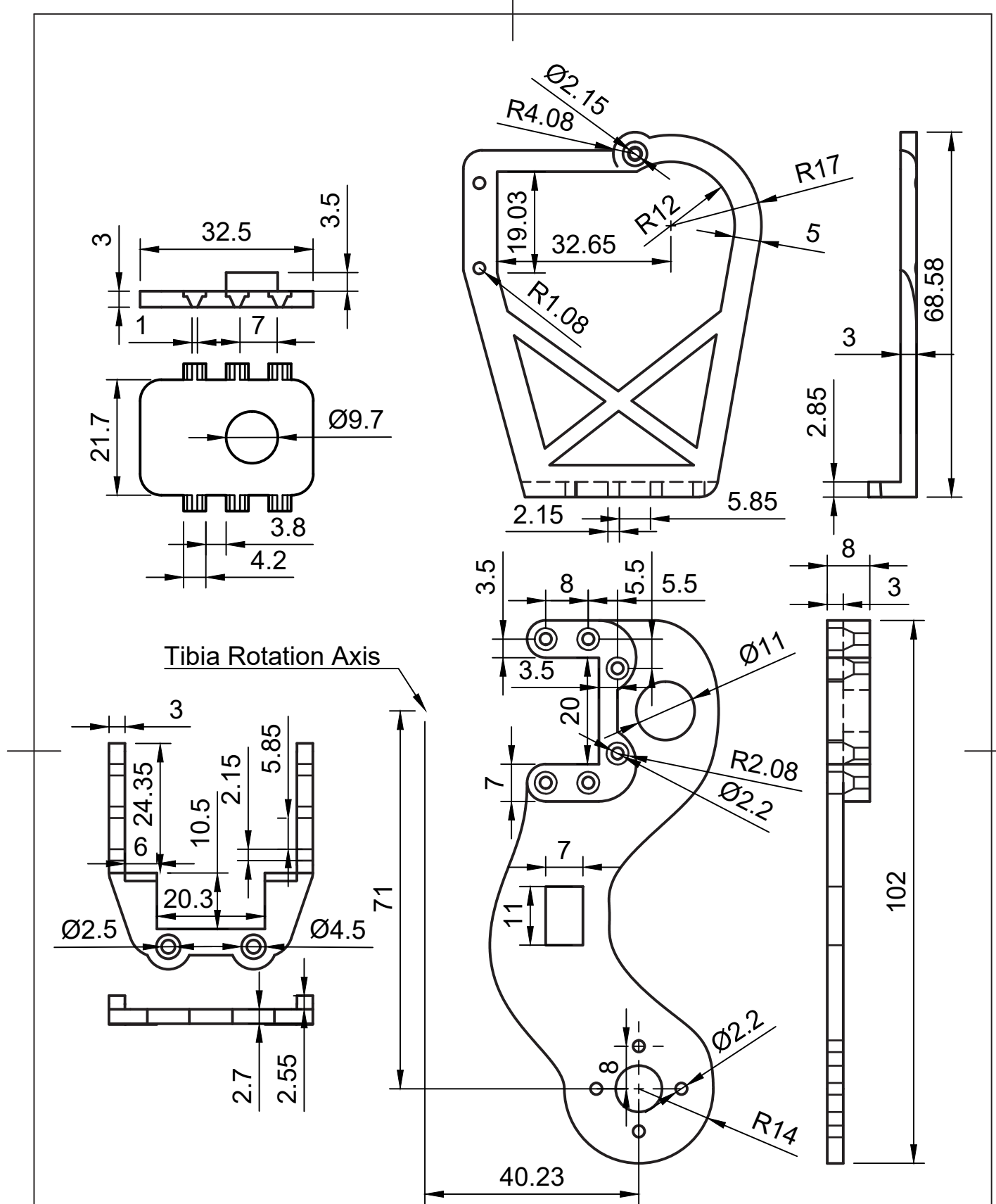
Dept. ComRob	Scale 1:1	Created by Martin Zoula, 10.5.2019	Approved by
		Document type <b>Technical Documentation</b>	Document status
		Title <b>HAntR Hexapod Robot Mechanical Design Body Plate</b>	DWG No.
	<b>FACULTY OF ELECTRICAL ENGINEERING CTU IN PRAGUE</b>	Rev. 1	Date of issue 24.5.2019
			Sheet 2/6



Dept. ComRob	Scale 1:1	Created by Martin Zoula, 10.5.2019	Approved by
		Document type <b>Technical Documentation</b>	Document status
		Title <b>HAntR Hexapod Robot Mechanical Design Batterypack Plate Dynamixel AX-12A</b>	DWG No.
		Rev. 1	Date of issue 24.5.2019
			Sheet 3/6



Dept. ComRob	Scale 1:1	Created by Martin Zoula, 10.5.2019	Approved by
		Document type Technical Documentation	Document status
		Title HAntR Hexapod Robot Mechanical Design Servo Facing Coxa Bracket	DWG No.
	<b>FACULTY OF ELECTRICAL ENGINEERING CTU IN PRAGUE</b>	Rev. 1	Date of issue 24.5.2019



Dept.  
ComRob

Scale  
1:1

Created by  
Martin Zoula, 10.5.2019

Approved by

Document type  
Technical Documentation

Document status

Title  
HAntR Hexapod Robot  
Mechanical Design  
Troch. Knob; Troch. Hoop  
Troch. Hoof; Femur Clamp

DWG No.

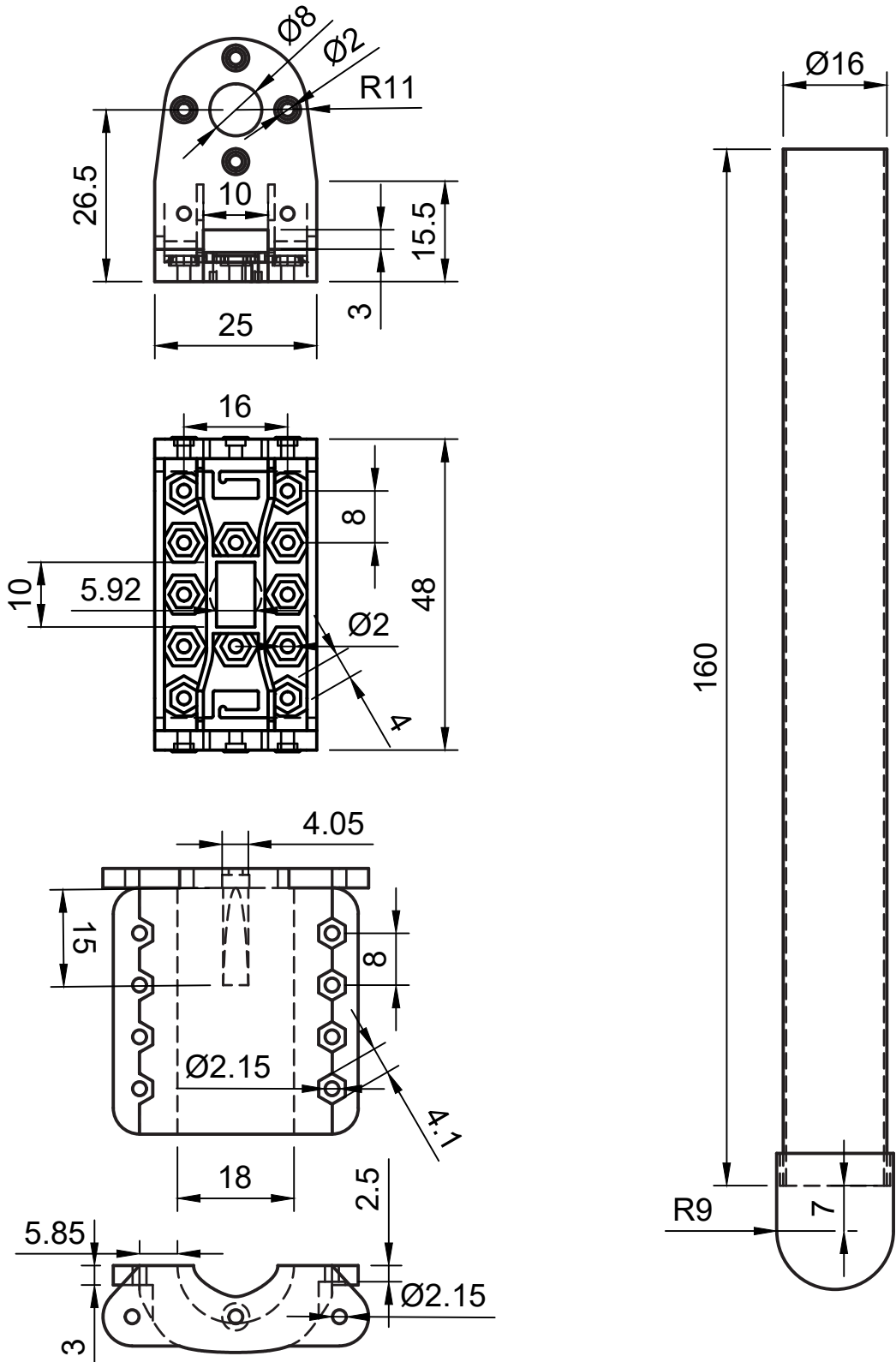
Rev.  
1

Date of issue  
24.5.2019

Sheet  
5/6



**FACULTY  
OF ELECTRICAL  
ENGINEERING  
CTU IN PRAGUE**



Dept. ComRob	Scale 1:1	Created by Martin Zoula, 10.5.2019	Approved by
 <b>FACULTY OF ELECTRICAL ENGINEERING CTU IN PRAGUE</b>		Document type <b>Technical Documentation</b>	Document status
Title <b>HAntR Hexapod Robot Mechanical Design Tibia Mount; Tibia Tube Foottip; Bioloid F2 Bracket</b>		DWG No.	
Rev. 1 Date of issue 24.5.2019		Sheet 6/6	

## **Appendix B**

# **Contents of Attached CD**

Following files and directories can be found in Compact Disk attached to this thesis.

- `zoulamar_bc_thesis.pdf` A digital copy of this thesis.
- `Appendix_A` A directory containing files related to Appendix A.
  - `design_drawing.pdf` PDF file containing attached documentation.
  - `STL_files.zip` A zip archive containing STL files of mechanical parts.
- `figures.zip` A zip archive containing fullscale figures used in this thesis.
- `src.zip` A zip archive containing C++ source files for experiment reproduction.